

Microclimate spatio-temporal prediction using deep learning and land use data

Han Jintong^a, Adrian Chong^{a,*}, Joie Lim^a, Savitha Ramasamy^b, Wong Nyuk Hien^a and Filip Biljecki^{c,d}

^aDepartment of the Built Environment, College of Design and Engineering, National University of Singapore, 4 Architecture Drive, 117566, Singapore

^bInstitute for Infocomm Research, Agency for Science, Technology and Research (A*STAR), 138632, Singapore

^cDepartment of Architecture, College of Design and Engineering, National University of Singapore, 4 Architecture Drive, 117566, Singapore

^dDepartment of Real Estate, Business School, National University of Singapore, 15 Kent Ridge Drive, 119245, Singapore

ARTICLE INFO

Keywords:

Microclimate Prediction
Interpolation
LSTM
Kriging
Urban morphology

ABSTRACT

Urban microclimate prediction is crucial for various fields, including Building Performance Simulation (BPS), outdoor thermal comfort, building life cycle, and residential health. Existing methods involve using classical weather file data, such as Typical Meteorological Years (TMY), or machine learning techniques for time-based forecasting. However, the incorporation of both spatial and temporal dimensions and land use/land cover (LULC) data is seldom considered. This paper proposes a novel approach to predict microclimate: the Geo-LSTM-Kriging model, which is applicable for fine-scale microclimate prediction within a few hundred meters around weather stations. The Geo-layer processes and learns from LULC data, the LSTM layer learns from historical data, and the Kriging layer extracts spatial distance information. This comprehensive combination integrates spatial, temporal, and environmental conditions, providing accurate results with higher spatial resolution (1 m × 1 m) and shorter time intervals (10 min). These prediction results were achieved by employing statistical downscaling calculation and utilizing data from 14 weather stations located within our university campus. Upon the analysis of these prediction results, we found that the proposed model can accurately predict temperature and humidity at high spatial and temporal resolution. Compared to traditional interpolation models, the RMSE of temperature decreases from 1.59 °C to 0.64 °C, and the RMSE of relative humidity (RH) decreases from 7.70 to 3.23. A thorough analysis of the model prediction results reveals the varied impacts of different LULC features on microclimate predictions, highlighting the value of the proposed model and the importance of incorporating LULC data.

1. Introduction

The proportion of the world's population in urban areas has increased significantly over the past decade. It is predicted to exceed 70% by 2050, according to a report by the United Nations (United Nations, 2019). Built environment and human activity have led to the urban heat island (UHI) effect (Arnfield, 2003; Akbari, Cartalis, Kolokotsa, Muscio, Pisello, Rossi, Santamouris, Synnefa, Wong and Zinzi, 2016; Chakraborty, Sarangi and Lee, 2021). This effect leads to higher temperatures compared to less urbanized areas, significantly contributing to global warming, heat-related deaths, and unpredictable climate variations (Deilami, Kamruzzaman and Liu, 2018). Recently, there has been an increased interest in research investigating the relationship between human activities and the surrounding environment, in an attempt to mitigate the UHI effect that negatively affects the built environment and its climate. Urban microclimate, pertaining to the immediate atmospheric conditions surrounding buildings distinguished from the broader urban climate (Wang, Li, Guo, Ma, Feng and Bao, 2021), has gained significant attention in this regard (Yang, Wang, Stathopoulos and Marey, 2023).

Previous studies have utilized experimental and mathematical methods to demonstrate how microclimate features (e.g. temperature, humidity) influence building energy systems (Bijarniya, Sarkar and Maiti, 2020; Im, Srinivasan, Maxwell, Steiner and Karmakar, 2022), including air conditioning systems and solar power systems (Bevilacqua,

*Corresponding author

✉ jintong@nus.edu.sg (H. Jintong); adrian.chong@nus.edu.sg (A. Chong); joie.lim@nus.edu.sg (J. Lim); ramasamysa@i2r.a-star.edu.sg (S. Ramasamy); bdgwnh@nus.edu.sg (W.N. Hien); filipt@nus.edu.sg (F. Biljecki)
ORCID(s): 0009-0002-8394-6290 (H. Jintong); 0000-0002-9486-4728 (A. Chong); 0000-0002-4893-211X (J. Lim); 0000-0003-1534-2989 (S. Ramasamy); 0000-0003-2964-7492 (W.N. Hien); 0000-0002-6229-7749 (F. Biljecki)

Morabito, Bruno, Ferraro and Arcuri, 2020; Wu, Hou, Hui, Tang and Wang, 2022). In the outdoor thermal comfort field, Zhang, Zhang, Gou and Liu (2022b) confirmed that microclimatic factors have a similar impact on outdoor thermal comfort as macroclimate factors, and therefore microclimate factors are particularly important for outdoor thermal comfort in regions with disadvantageous macroclimates. Some studies have explored the impact of various parameters within microclimates on the physical health of residents (Wu, Liu, Li and Yin, 2020; Heidari, Mohammadbeigi, Khazaei, Soltanzadeh, Asgarian and Saghafipour, 2020). Hayles, Huddleston, Chinowsky and Helman (2022) found that the microclimate changes in precipitation and humidity have a significant impact on the service life of building materials. Gaining accurate knowledge and predicting various indicators of local microclimates can be beneficial for extensive research on microclimate impacts. In summary, characterizing the local microclimate has different applications in improving building performance, building material life-cycle, occupant health, and thermal comfort. Under constantly changing climate conditions, the prediction of microclimates becomes increasingly crucial.

However, various features of the microclimate may exhibit significantly different performances and drastic fluctuations within a very small spatial and temporal range. In Figure 1, we have compiled the changes in temperature and humidity for one hour from 14 weather stations within the scope of this study, which is a $1.9\text{ km} \times 1.6\text{ km}$ urban area, as shown in Figure 2. The data represent the statistical results of minute-by-minute data within one hour. In Figure 1, the red numbers represent the standard deviation of temperature and humidity among different weather stations within one hour. We can observe fluctuations not only between adjacent weather stations, but also within the same station, with standard deviations of temperature reaching approximately $2\text{ }^{\circ}\text{C}$ and standard deviations of RH reaching 7% within one hour. However, existing research on microclimate prediction often overlooks this aspect. There are two relatively obvious gaps here: (1) the lack of microclimate data at high spatial and temporal resolution; (2) the need for more targeted predictions by incorporating contextual spatial data such as land use/land cover (LULC). Meanwhile, many studies have demonstrated the influence of LULC on microclimate data. Estoque, Murayama and Myint (2017) demonstrated that the mean temperature of the impervious surface is about $3\text{ }^{\circ}\text{C}$ higher than that of the green space. However, there is still a lack of research that integrates land use in predicting the urban microclimate indicators at high spatial and temporal resolution. Therefore, this paper has the following two objectives:

- To provide downscaling temperature and humidity data at a high spatial resolution and short temporal intervals that are sufficient for micro-climate-related studies.
- To develop a model that considers the surrounding environmental conditions and further enhances the model performance based on existing algorithms.

To achieve the aforementioned objectives, this paper proposes a Kriging-based LSTM neural network model combined with geographical land use data, which is called Geo-Kriging-LSTM, to estimate temperature and RH for the locations without weather stations or sensors. The rest of the paper is organized as follows: in Section 2, an extensive examination of previous studies on microclimate prediction is presented, encompassing a range of methodologies. Section 3 illustrates the structure of the model and the inferences of the network, including the overview and verification of the data sources. Then in Section 4, the experiment results are displayed and evaluated. Sections 5 and 6 discuss the significance and conclude this study.

2. Related Work

In this section, we will provide existing research relevant to the following two main aspects: the impact of microclimate data on a wide range of studies and commonly used microclimate prediction methods. Among these prediction methods, they are categorized into temporal methods, spatial methods, and combined spatio-temporal methods.

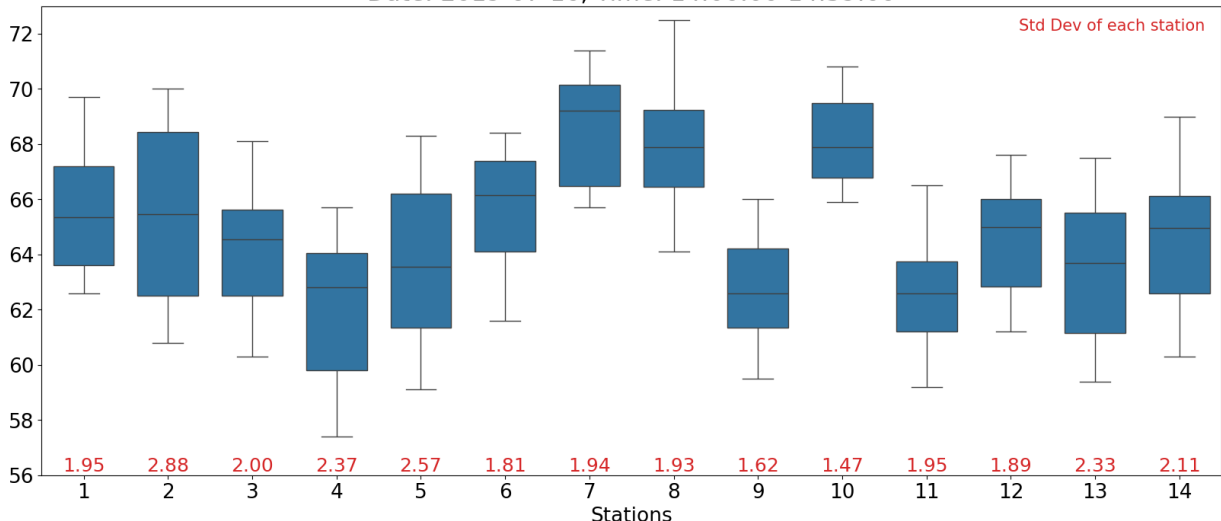
2.1. Impact of microclimate

Studying and predicting the variation of the urban microclimate variables in space and time is vital for various studies. In building performance simulation, weather data form the boundary condition for energy calculations and daylight analysis. Existing studies often utilize typical weather files such as the Weather Year for Energy Calculation 2 (WYEC2) and the Typical Meteorological Year (TMY) (Han, Ang, Malkawi and Samuelson, 2021). However, typical weather files lack a precise depiction of the microclimate conditions specific to the local area. Past studies have highlighted notable distinctions in temperature, humidity, and other variables between weather files data, urban

Microclimate spatio-temporal prediction

RH (%) distribution over stations, and RH Std Dev of each station.

Date: 2019-07-16, Time: 14:00:00-14:59:00



Temperature ($^{\circ}\text{C}$) distribution over stations, and Temperature Std Dev of each station.

Date: 2019-07-16, Time: 14:00:00-14:59:00

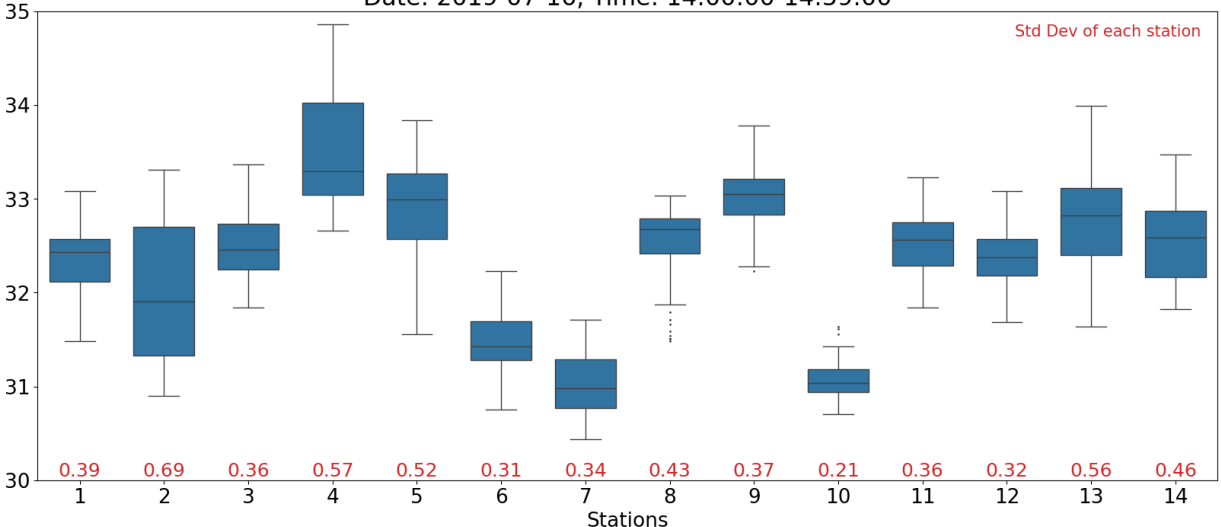


Figure 1: Temperature and Relative humidity changes within one hour in the research area.

climate stations, and adjacent microclimate stations (Wang et al., 2021; Lazos, Sproul and Kay, 2014). Hosseini, Lee and Vakilinia (2017) undertook an extensive building performance simulation to investigate the impact of weather uncertainty on building energy estimation in Montreal, Canada, showing variances ranging from 3% to 29% in energy consumption when comparing simulations using actual weather data versus TMY2 data.

In the field of outdoor thermal comfort, Zhang et al. (2022b) confirmed that microclimate factors have a similar impact on outdoor thermal comfort as macroclimate factors. Vinayak, Lee, Gedam and Latha (2022) revealed that future increases in temperature in microclimates could result in 20% Mumbai Metropolitan Region experiencing outdoor thermal discomfort. Lin and Brown (2021) determined that incorporating microclimate information into urban landscape design can create outdoor environments with enhanced thermal comfort. Zhang, Li, Wei and Hu (2022a) explored the interaction mechanism among building spatial morphology, urban microclimate, and thermal comfort, indicating that geographical factors, such as urban vegetation, further influence outdoor thermal comfort by affecting various microclimate characteristics.



Figure 2: The positions of weather stations whose data are used in model training, together with street-level imagery showing the streetscape in the study area.

Microclimate conditions also have an impact on different facets, such as residents' health. Schinasi, Benmarhnia and De Roos (2018) summarized the association between microclimate indicators and epidemiology, and found that people living in hotter areas within cities had a 6% higher risk of mortality/morbidity compared to those in cooler areas. Zeren Cetin, Varol and Ozel (2023) demonstrated a strong positive correlation between microclimate indices, particularly land surface temperature (LST), sleep deprivation, and heat stress among residents. Alimukhamedov et al. (2022) assessed the health effects of microclimate indices on workers and finds that these conditions have a greater impact on male workers than on female workers. Moreover, adverse microclimate conditions have varying degrees of influence on the cardiovascular, respiratory, and urinary systems of both genders.

Therefore, having accurate knowledge and predicting various indicators of local microclimate is beneficial for extensive research on microclimate. From the references above, we can also observe that wind speed, mean radiant temperature, air temperature and humidity are widely employed indicators in microclimate analysis. This study will focus on two of them, which are air temperature and relative humidity.

2.2. Microclimate prediction methods

In macroscopic terms, microclimate prediction methods can be categorized into three main types: methods that utilize historical data for temporal prediction, methods that use neighboring spatial data for prediction, and hybrid methods that combine both temporal and spatial data for prediction.

2.2.1. Temporal prediction methods

The majority of microclimate prediction methods are based on historical data. To anticipate the characteristics of the urban microclimate, the prevailing approach often involves two categories: mathematical modeling, including Numerical Weather Prediction (NWP) models, and artificial neural network approaches. Employing mathematical

modeling techniques often encompasses mass and energy balances. Quemada-Villagómez, Miranda-López, Calderón-Ramírez, Navarrete-Bolaños, Martínez-González and Jiménez-Islas (2021) put forward a straightforward mathematical model aimed at estimating the annual maximum and minimum daily environmental temperatures. Such generalized mathematical models often have limitations in their ability to predict within larger spatial scales, and their predictions typically represent characteristic values, such as maximum or minimum values, over a given period. NWP models are built upon the fundamental principles of weather physics and account for the boundaries and environmental conditions associated with weather phenomena (Mathiesen and Kleissl, 2011). NWP is capable of providing more accurate and detailed predictions, but it comes with the trade-off of higher computational costs to model the atmospheric system (Aggarwal and Kumar, 2013). Di Napoli, Hogan and Pappenberger (2020) used NWP to predict global-scale mean radiation temperature (MRT). Within the scope of microclimate, their study obtained weather data predictions with a spatial resolution of 2.5×2.5 km using NWP. However, for more detailed investigations into building performance or outdoor thermal comfort, the spatial resolution is insufficient.

Alternatively, with the rapid development of artificial intelligence technology, machine learning methods are increasingly being applied in microclimate prediction. These methods commonly used can be broadly categorized into two types: Feed-forward Neural Networks (FFNN) and Recurrent Neural Networks (RNN). FFNN are data-driven predictive models that rely on data to capture and represent complex, non-linear patterns in large-scale weather datasets. Bile, Tari, Grinde, Frasca, Siani and Fazio (2022) utilized FFNN to predict the short-term temperature trends inside museums, aiming to provide preventive measures for the protection of cultural artifacts. Xie, Ishida, Hu and Mochida (2022) applied an FFNN model to predict the mean radiant temperature surrounding buildings. FFNNs offer benefits such as reproducibility, time-efficiency, and scalability, allowing them to be easily adapted to different temporal resolutions (Mocanu, Mocanu, Stone, Nguyen, Gibescu and Liotta, 2018). RNNs are designed for time series data, and they have the ability to capture temporal dependencies and retain information from historical data. In addition to the basic RNN architecture, LSTM (Long Short-Term Memory) is another type of network developed based on RNN, and GRU (Gated Recurrent Unit) is a further simplified network based on LSTM (Zargar, 2021). Zhang, Zhang, Guo, Xu, Chen and Wang (2021) used Long Short-Term Memory (LSTM) models for microclimate prediction and investigated their influence on buildings with different geometric configurations. Koc and Acar (2021) used LSTM to predict temperature, showcasing the effectiveness of LSTM for climate prediction. However, research on utilizing RNNs for climate prediction studies is still relatively nascent in the built environment-related domains (Han et al., 2021).

2.2.2. Spatial prediction methods

There are various methods for spatial microclimate prediction. In general, researchers typically use standard weather file data as a baseline and employ different methods for downscaling calculations. There are two main approaches to downscaling weather data files: dynamical and statistical downscaling. The dynamical downscaling approach involves the utilization of physical models to simulate future weather, yielding data with higher resolution and enhanced reliability. Computational Fluid Dynamics (CFD) models are commonly used to simulate wind flow in urban areas, which can resolve the transfer of heat and mass and their interaction with individual obstacles, such as buildings (Topalar, Blocken, Maiheu and Van Heijst, 2017). With the development of CFD and other physical-based microclimate models, an increasing number of studies have employed these models as predictive methodologies. Crank, Sailor, Ban-Weiss and Taleghani (2018) tested the air temperature perturbations using ENVI-met (a high-resolution 3D microclimate simulation software) with different vertical grid resolutions (0.75 to 2.0 m) and found that ENVI-net performs robustness when changing vertical resolution. Maronga, Gryschka, Heinze, Hoffmann, Kanani-Sühring, Keck, Ketelsen, Letzel, Sühring and Raasch (2015) algorithmically optimized the Parallelized Large-Eddy Simulation Model (PALM), enabling it to perform computationally intensive simulations of meteorological data at large spatial scales and very high grid resolutions. Moradi, Dyer, Nazem, Nambiar, Nahian, Bueno, Mackey, Vasanthakumar, Nazarian, Krayenhoff et al. (2021) adopted and validated the Vertical City Weather Generator (VCWG) model (an efficient urban microclimate physics model) to assess its predictive performance within urban area, they found that the model is capable of accurately forecasting temperature, humidity, wind speed, and other variables in a three-dimensional space. We can observe that such physics-based models generally exhibit higher accuracy and a denser spatial resolution. However, it is equally true that, being based on physics-based meteorological models, they often require higher computational costs and a more accurate representation of topographical conditions within the specific scope (P. Tootkaboni, Ballarini, Zinzi and Corrado, 2021).

On the other hand, the statistical downscaling is a simpler approach that establishes statistical connections between observed local climate variables and large-scale climate variables Bamdad, Cholette, Omrani and Bell (2021). Although statistical downscaling has the advantage of computational speed, its accuracy may be inferior compared to the computationally intensive dynamical downscaling method. Aliabadi and McLeod (2023) introduced the Vatic Weather File Generator (VWFG), a model capable of predicting weather conditions for the next 80 years based on records from the past 20 years. The ability to generate long-term future weather files aids in forecasting the energy consumption demands for heating and cooling in urban buildings. As illustrated in their study, such statistical downscaling methods typically rely on archives of TMY data, which are then adjusted based on commonly used regional or global climate models. These methods are more commonly employed for long-term climate trend predictions, lacking a perspective on shorter time intervals, and exhibiting a higher dependency on climate models and weather files. Meanwhile, we observe that interpolation methods are seldom mentioned in downscaling approaches, despite their ability to utilize localized meteorological station data for more direct and targeted downscaling computations.

Traditional spatial interpolation techniques can generally be categorized into deterministic methods (such as Triangular-based interpolation (Watson and Philip, 1984), Inverse Distance Weighted (IDW) (Bartier and Keller, 1996), and Trend Surface Analysis (TSA) (Agterberg, 1984), Spline interpolation (Schoenberg, 1973)), geostatistical methods (such as Kriging), and hybrid methods (such as Regression Kriging) (Granville, Woolford, Dean, Boychuk and McFayden, 2023). In traditional interpolation methods, the most commonly used ones are IDW, Kriging, and Regression Kriging (RK) (Li and Heap, 2011). Among them, Regression Kriging is the combination of multivariate regression and Kriging and has been proven to have better interpolation performance in numerous instances. Meng, Liu and Borders (2013) compared seven GIS interpolation methods and demonstrated that RK has the potential to significantly improve spatial prediction accuracy even when using a weakly correlated auxiliary variable. Gia Pham, Kappas, Van Huynh and Hoang Khanh Nguyen (2019) used different interpolation methods to estimate soil properties and observed that RK and Kriging exhibited respective advantages in various components, yet RK demonstrated superior performance in a majority of scenarios. Azawi and Saleh (2021) used different interpolation methods to estimate groundwater quality and found that RK yields higher accuracy.

Some other studies also applied machine learning methods to interpolation models. Kartal (2022) designed a hybrid method that combines the spatial interpolation approach with artificial neural networks, achieving MAE of 2.85 °C using their NN-ConcLSTM model. Imanian, Shirkhani, Mohammadian, Hiedra Cobo and Payeur (2023) used deep learning approaches to overcome the weakness of the spline method when predicting the land-water interface temperature, reducing the RMSE by 16.2%.

We can observe that in addition to traditional interpolation methods, most recent studies choose to combine spatial interpolation with machine learning models to address the demand for higher spatial resolution. In this study, we combine spatial interpolation with time-series prediction and also utilize the assistance of RNN models to achieve the same goal. The classic and broadly applied interpolation methods mentioned above will serve as baselines in this study. In summary, we utilized the machine learning methods with the incorporation of both temporal and spatial information.

2.2.3. Incorporating land use/land cover (LULC)

Land use/land cover (LULC) has been of great importance worldwide for many years. Land use encompasses the themes, purposes, duration, and spatial aspects of land utilization, while land cover primarily includes the types and properties of surface features on land (Nedd, Light, Owens, James, Johnson and Anandhi, 2021). Many studies have demonstrated the significant impact of LULC on urban microclimate indicators. With the rapid development of human society, the influence of LULC on microclimate is increasing and shows no signs of diminishing due to the incrementally active, diverse, and internationalized human activities (Caballero, Ruhoff and Biggs, 2022; Naikoo, Islam, Mallick, Rahman et al., 2022; Abdullah, Barua, Abdullah and Rabby, 2022). Zhang et al. (2022a) investigated the impact of LULC on microclimate and found a strong correlation between temperature, humidity, and specific building morphology parameters such as sky view factor, floor area ratio, site coverage ratio, and building storeys (Wei, Song, Wong and Martin, 2016). Erell and Zhou (2022) found using microclimate simulations that increasing vegetation coverage can lead to a decrease of 0.3 °C in annual average temperature. Consequently, incorporating LULC data in microclimate predictions could improve prediction performance. Chang, Lam, Lau and Wong (2021) employed data-driven machine learning techniques in conjunction with LULC data to develop a 50 × 50 m grid-based temperature forecast for extreme events on the Kowloon Peninsula in Hong Kong, their results show that the statistical downscaling process reduced the model MAE by 1.03 °C to 0.3 °C for the maximum and minimum local temperature prediction. Ma, Ding, Cheng, Jiang and Wan (2019) introduced a novel spatial interpolation/extrapolation

methodology, called Geo-LSTM, to produce the spatial distribution of air pollutant concentrations, which integrates the spatial-temporal correlation from other monitoring stations. However, there is still a scarcity of studies integrating LULC for microclimate prediction, especially for studies requiring high spatial resolution microclimate data, which necessitates further research.

3. Methodology

The method employed in this study consists of four main steps, which we elaborate on in the subsequent subsections.

1. Data preparation and verification (Section 3.1).
2. Model construction: Establishing the model structure based on representative RNN networks and interpolation methods. The proposed algorithm will be described in Section 3.2 and 3.3.
3. Performance evaluation: Performance comparisons with baselines (classical RNNs and interpolation methods). The detailed exposition of these comparisons will be presented in the first two subsections of Section 4.
4. Incorporation of LULC data and its impacts: Having confirmed and selected the most promising machine learning models, we proceeded to incorporate the LULC data and conducted a comprehensive analysis of its impact on the model outcomes. A detailed exposition of this investigation will be provided in the last two subsections of Section 4.

3.1. Data preparation and verification

The dataset utilized for training and testing in this study comprises 14 weather stations on the ground, which are located at the National University of Singapore (1.2955 N, 103.777 E). The geographical distribution of these stations is depicted in Figure 2, spanning an area of approximately 1.9 km × 1.6 km.

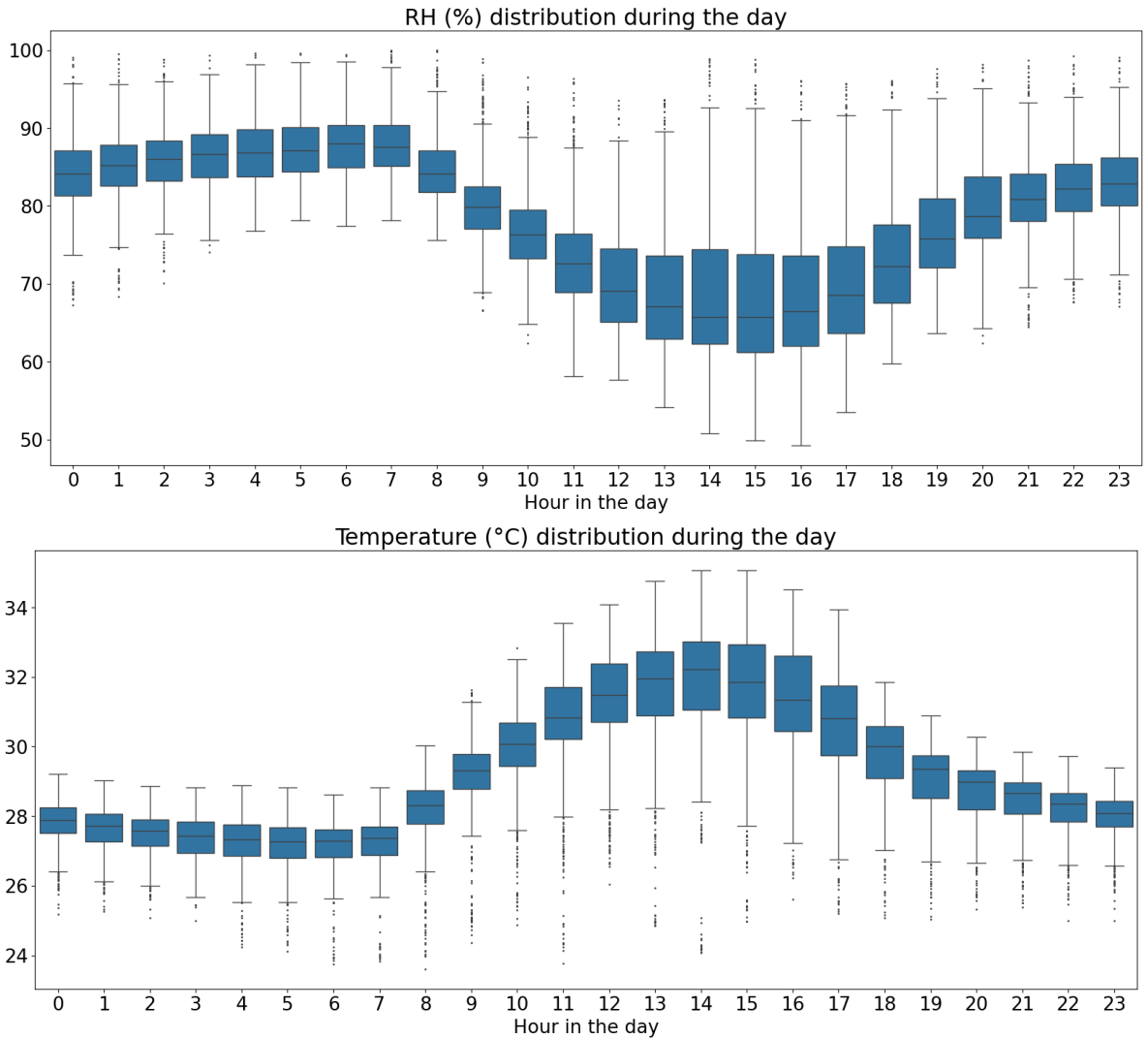
This study uses data collected over a month (July 2019) with a sampling interval of 1 minute, including 44,640 records for each station. As shown in Figure 4, the measurement of temperature and RH was conducted using the ONSET S-THB-M00x temperature/RH smart sensors installed at a 2.4 m height, restricted by NUS campus safety regulations. Specifications for the sensors are listed in Table 1. The computational results presented in this article are all based on the resolution of sensor readings, which are retained to two decimal places. Each temperature sensor was positioned consistently, ensuring a distance of more than 20 cm from the solar panel to prevent overheating. A cloud-based platform was established to facilitate remote data collection and monitoring via a 3G wireless connection. We also compiled the overall humidity and temperature data for the month of July 2019 from these 14 weather stations. The average temperature for the entire month is 28.0 °C, with a standard deviation of 2.06 °C, and the average RH is 83.2%, with a standard deviation of 9.76%. The time series statistics of the raw data for temperature and humidity for the given month are shown in Figure 3. The horizontal axis represents the hours of the day, and the vertical axis represents the humidity and temperature measured by the weather stations. A general observation indicates significant fluctuations in the measurement values during the daytime, with higher temperatures and lower humidity. In the subsequent analysis of the prediction results, we will provide a more detailed examination in conjunction with the actual data performance.

Table 1
Specifications of environmental sensors.

Parameter	Range	Accuracy	Resolution
Temperature	-40 °C-75 °C	±0.21 °C	0.01 °C
Solar Radiation	0-1280 W/m ²	±10 W/m ²	1.25 W/m ²

One month of data is deemed to be sufficient for this research because many of the climate variables in Singapore, such as temperature and relative humidity, do not show significant month-to-month variation. To illustrate this, we compute the Kullback–Leibler (KL) divergence between the distribution of one-month data and the entire year. KL-divergence, as defined by Kullback and Leibler (1951), is a statistical measurement from information theory that measures differences in information represented by two distributions. The results are summarized in Table 2.

When we attempt to fit a relatively complex distribution that we have observed with a simpler and common distribution (e.g. uniform distribution, binomial distribution), there may be a loss of information due to the discrepancy between the fitted distribution and the observed distribution. Kullback-Leibler (KL) divergence is introduced to measure the information loss and quantify the discrepancy between two probability distributions. The formula of

**Figure 3:** The time series distribution of measures RH and Temperature.**Table 2**

KL divergence. P denotes the distribution over the whole year. Q denotes the distribution of data collected in July 2019. U denotes the uniform distribution. N denotes the normal distribution with the same mean and standard deviation as the whole year data.

Weather feature	$KL(P Q)$	$KL(Q P)$	$KL(P U)$	$KL(P N)$
RH	0.1734	0.1443	0.4406	0.1571
Temperature	0.1679	0.1489	0.3616	0.1280

computing the $KL(P||Q)$ is shown as Equation 1. From Table 2, it is evident from Table 2 that the $KL(P||N)$ is minimal, which shows that the data from July 2019 have a distribution similar to that of the whole year.

$$KL(P||Q) = \sum_x P(x) \log \left(\frac{P(x)}{Q(x)} \right) \quad (1)$$

LULC classification is a systematic and complex study area. In traditional research, such data are often used for purposes like urban planning and construction over larger areas. The classification of LULC generally includes forests, farmlands (of different crops), lands, buildings, roads, water sources, and so on (Hütt, Koppe, Miao and Bareth, 2016; Vivekananda, Swathi and Sujith, 2021). The classification of LULC can also be flexibly adjusted based on the research field and objectives (Gaur and Singh, 2023). In this small-scale microclimate study paper, considering the actual conditions of the research site, we primarily categorized LULC into the following types: distance to buildings, percentage covered by buildings, terrain (the height above sea level in meters), vegetated area, temporary area, urban canyon, distance to trees, distance to walkways, distance to roads, distance to paths, distance to court tracks, distance to car parks, percentage of road, percentage of paths, percentage of walkway, percentage of court tracks, percentage of car park, and number of trees. After applying a random forest regressor sensitivity analysis on a trial dataset, we select the 8 most important features, which are distance to buildings, distance to trees, distance to walkways, distance to roads, distance to paths, distance to court tracks, distance to car parks, and terrain. The values of the 8 features of LULC are derived from urban morphology data collected on the GIS map and buildings' 3D models of the NUS campus. The urban morphology data used in our study are in vector format, allowing us to choose an appropriate resolution based on our needs for high spatial resolution. The LULC data used in this study is collected on resolution grid of 1 m, ensuring high spatial density and providing more detailed geographical information.



Figure 4: Example weather stations used in this study.

3.2. Variable notations

Before delving into the detailed description of the model network structure, we will first introduce the relevant variables and their abbreviations in this section.

Given a time sequence of weather data after processing $\mathbf{X} = [x_1, x_2, \dots, x_{T-1}, x_T]$ with the time length T , where x_t denotes the weather data information at time t . This model is used to estimate the weather data at time t of the target position \mathbf{S}^0 , where $x_t \in \mathbb{R}^{N \times M}$ represents the observed value of M weather features of N weather stations, as shown in Equation (2).

$$x_t = \begin{bmatrix} x_t^{1,1} & x_t^{1,2} & \dots & x_t^{1,M} \\ x_t^{2,1} & x_t^{2,2} & \dots & x_t^{2,M} \\ \vdots & \vdots & \ddots & \vdots \\ x_t^{N,1} & x_t^{N,2} & \dots & x_t^{N,M} \end{bmatrix} \quad (2)$$

In the case here, there are 2 features, i.e. $M = 2$. For convenience, we use *tem* to denote the temperature and *rh* to denote the relative humidity respectively.

To take the spatial information into concern, Equations (3) and (4) show the coordinates of the stations in the local coordinate system.

$$\mathbf{s} = [s^1, s^2, \dots, s^N] \quad (3)$$

$$s^i = [CoordX^i, CoordY^i] \quad (4)$$

The LULC data input is given for training use as the following Equation (5)

$$\mathbf{g} = [g^1, g^2, \dots, g^N] \quad (5)$$

Here g^i is an 8-dimensional vector that contains the 8 LULC features used in the Regression Kriging model, these features are ‘terrain’, ‘distance to building’, ‘distance to tree’, ‘distance to walkway’, ‘distance to road’, ‘distance to path’, ‘distance to court track’, and ‘distance to car park’.

Combining the above equations, there are three parts of inputs in our model. Except for the LULC information g^0 , we also need the target position $s^0 = [CoordX^0, CoordY^0]$ and time series weather data of the stations, $[x_{t-r+1}, x_{t-r+2}, \dots, x_t]$, where t is the target time, r is a hyperparameter representing the length of the time window. Our target output is $[tem_t^0, rh_t^0, vx_t^0, vy_t^0]$, which represents the weather features of the target position.

3.3. Model architecture design

The proposed model architecture is founded upon the fusion of using Long Short Term Memory (LSTM) to model temporal correlations and the Kriging model to model spatial correlations.

The proposed network architecture comprises three primary components: the geographical layer, the Kriging layer, and the LSTM layer. The geographical layer integrates geographic information with observed station data, while the Kriging layer estimates time series data for the target location. The LSTM layer processes the temporal information of the time series data. The interconnections between the three layers are illustrated in Figure 5.

3.3.1. Geographical layer

The geographical layers serve as filters for weather data processing. In particular, they take the time series data \mathbf{X} and the LULC information represented in percentage form \mathbf{g} as inputs. These layers then utilize a set of weights $\mathbf{c} = [c^1, c^2, \dots, c^M]$ to adjust the weather features accordingly. The output of the geographical layer is computed using the following formula:

$$out_geo = \mathbf{X} * [\mathbf{g}\mathbf{c}^T + (1 - \mathbf{g})\mathbf{1}^T] \quad (6)$$

where $\mathbf{1} = [1, 1, \dots, 1] \in \mathbb{R}^{M \times 1}$. The output of the geographical layer is used as input data for the remaining part of the neural network. To maintain notation simplicity, we will continue to denote this output as X . Considering that the input \mathbf{g} represents the average value of the LULC information within the neighborhood, the geographical layer can be likened to a convolutional layer.

3.3.2. Regression Kriging layer

In Section 3.2, a sensitivity analysis and screening were conducted on the available LULC data, resulting in the identification of 8 significant features. This subsection will elaborate on the detailed application of these features in the model.

The Regression Kriging layer generates the weather feature data in the whole computing area. At each time, the weather feature x_t^0 is interpolated by the weather station data predicted by the LSTM layer, $x_t^1, x_t^2, \dots, x_t^M$. Using Regression Kriging, we obtain:

$$x_t^0(s^0) = \sum_{i=1}^N \mathbf{w}^i \cdot q_i(s^0) + \sum_{i=1}^M \lambda^i \cdot e(s^i) \quad (7)$$

where $\mathbf{w}^i = [w^{i,1}, w^{i,2}, \dots, w^{i,M}]^T \in \mathbb{R}^{1 \times M}$, representing the weights of the i th LULC features. The first term denotes the deterministic part of the model. λ^i are Kriging weights determined by the spatial dependence structure of the residual, and the second term interpolates the residual. These weights are the results generated from the Kriging layer.

In the Kriging method, we assume that the same type of weather data from all the weather stations has an identical distribution. In order to estimate the weights, we need to know the covariance between the weather data of two positions. Since LULC information has been considered in the geographical layer, a simpler model is used in the Kriging layer.

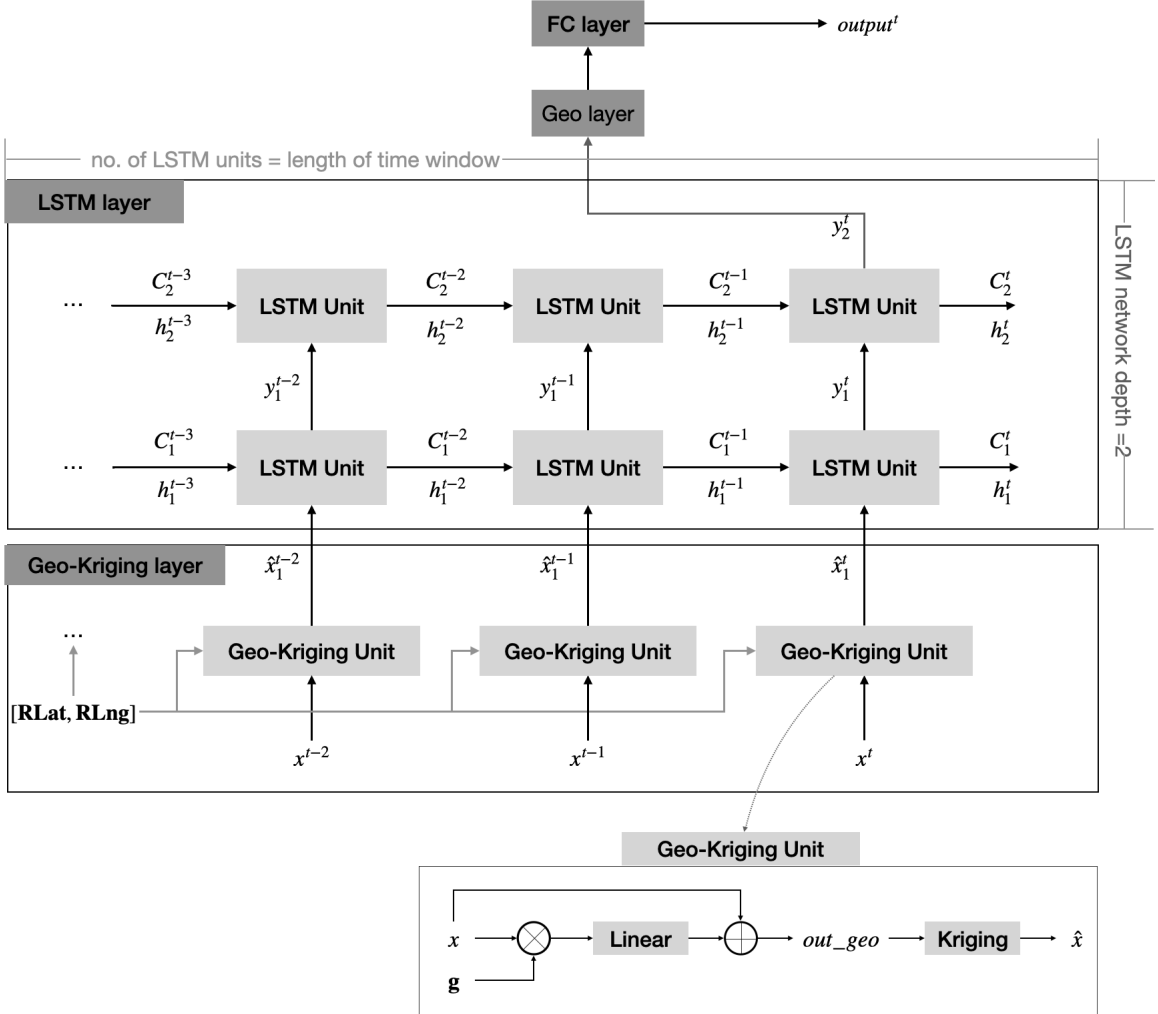


Figure 5: Diagram of Geo-Kriging-LSTM network structure.

We assume that the covariance is only dependent on the distance between two positions. In equal, we use the following equality to estimate covariance:

$$\text{Cov}(x_t^{i,k}, x_t^{j,k}) = \gamma^k(d^{ij}) \quad 1 \leq i, j \leq N; \quad 1 \leq k \leq M \quad (8)$$

where γ^k (for $1 \leq k \leq M$) are M functions to estimate the covariance of variables, and d^{ij} denotes the distance between station i and station j . There are several parameters in each function, and the parameters in γ^k will be learned in the network. In detail, we use the following ball correlation function: γ^k :

$$\gamma^k(d) = \begin{cases} b^k \left(1 - \frac{3}{2} \frac{d}{a^k} + \frac{1}{2} \left(\frac{d}{a^k} \right)^3 \right) & d \leq a^k \\ 0 & d > a^k \end{cases} \quad (9)$$

where a^k and b^k are the parameters that represent the maximal correlation distance and variance of the type of weather data respectively.

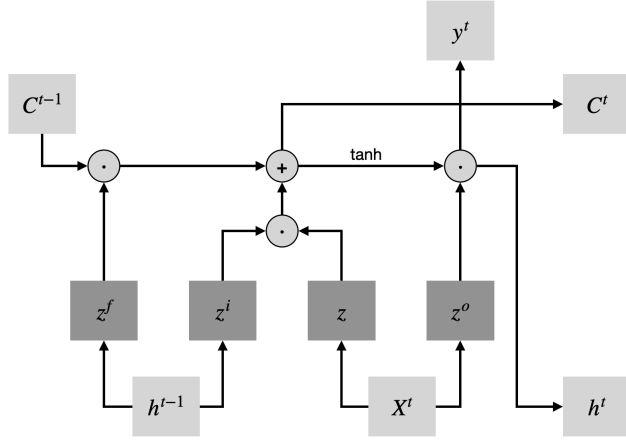


Figure 6: Mechanism of each LSTM unit.

Once the covariance is given, we can use the stochastic method to analyze that the optimal weights can be solved from the following linear equation system (10):

$$\begin{bmatrix} \gamma^k(d^{11}) & \gamma^k(d^{12}) & \dots & \gamma^k(d^{1N}) & 1 \\ \gamma^k(d^{21}) & \gamma^k(d^{22}) & \dots & \gamma^k(d^{2N}) & 1 \\ \vdots & \vdots & \ddots & \vdots & \vdots \\ \gamma^k(d^{N1}) & \gamma^k(d^{N2}) & \dots & \gamma^k(d^{NN}) & 1 \\ 1 & 1 & \dots & 1 & 0 \end{bmatrix} \begin{bmatrix} w^{1,k} \\ w^{2,k} \\ \vdots \\ w^{N,k} \\ \eta \end{bmatrix} = \begin{bmatrix} \gamma^k(d^{01}) \\ \gamma^k(d^{02}) \\ \vdots \\ \gamma^k(d^{0N}) \\ 0 \end{bmatrix} \quad (10)$$

where d^{0i} denotes the distance between target position and the station i , which is similar to the definition of d^{ij} . η is a Lagrange parameter used as an intermediate variable.

Once we know the value of Kriging weights, we can sum-product the weights and weather data together and get an estimation of the time series data for the target position. These time-series data will be the input of the LSTM layer. The mechanism of the Geo-Kriging layer could be found in the logical diagram of Geo-Kriging unit in Figure 5.

3.3.3. LSTM layer

Long Short-Term Memory (LSTM) (Hochreiter and Schmidhuber, 1997) is derived from the Recurrent Neural Network (RNN), which can process sequential data. LSTM controls the transmission states by four gates to the memory of important knowledge and releases the memory of unimportant information, to achieve a balance of learning speed and accuracy for time series data prediction. It has been broadly applied in various areas including speed recognition, translation, prediction, etc. (Van Houdt, Mosquera and Nápoles, 2020). Built environment data is a representative time series kind of data, especially weather data, which is highly correlated with changes in the time of day. Therefore, the LSTM is a good basic model for the weather interpolation task. However, the existing methods combined with LSTM can only predict the features with historical data. The model proposed in this paper combines the strength of LSTM and Kriging interpolation, to calculate the weather features for the locations without historical data.

As shown in Fig. 5, the data processed by the Geo-layer and Kriging layer will continue to pass through the LSTM layer, where the historical knowledge could be memorized by each LSTM unit. Fig. 6 shows the internal mechanism of each LSTM unit at time t . The hidden state of the last unit h_{t-1} , the cell state of the last unit c_{t-1} , together with the input data x_t form the inputs of each LSTM unit, processed by four different gates in LSTM. The f_t is the forgetting gate, represents the information of C_{t-1} after oblivion to calculate C_t , the C_t denotes the updated value of the unit state, calculated by the input data x_t and the hidden state h_{t-1} . The i_t is the input gate and the o_t is the output gate. The final o_T represents the output of the entire LSTM layer. In our model, T is set to 144, indicating the utilization of 24 hours of data for predicting data at 10-minute intervals within the next hour. These components work together to proceed to the LSTM layer. The detailed mathematical formula is listed in equations 11.

$$\begin{aligned}
f_t &= \sigma(W_f \cdot [h_{t-1}, x_t] + b_f) \\
C_t &= f_t \times C_{t-1} + i_t \times \tilde{C}_t \\
i_t &= \sigma(W_i \cdot [h_{t-1}, x_t] + b_i) \\
\tilde{C}_t &= \tanh(W_C \cdot [h_{t-1}, x_t] + b_C) \\
C_t &= f_t \times C_{t-1} + i_t \times \tilde{C}_t \\
o_t &= \sigma(W_o \cdot [h_{t-1}, x_t] + b_o) \\
h_t &= o_t \times \tanh(C_t)
\end{aligned} \tag{11}$$

3.4. Clustering methods for time series data

As the predicted results are all time series data, for a comprehensive analysis of time series results later in the text, common time series classification methods were employed in this study. There are many existing methods. Abanda, Mori and Lozano (2019) broadly categorized into three types: feature-based, model-based, and distance-based methods. Complex classification methods are suitable for higher-dimensional time series data. Therefore, for the task of classifying time series data in this paper, we adopted the classic dynamic Time Warping (DTW) algorithm. It is widely appreciated for its efficiency in measuring similarity between time series, effectively mitigating the impacts of time shifts and distortions. It achieves this by enabling a flexible transformation of time series, allowing the detection of similar shapes even with different phases (Senin, 2008).

Simultaneously, for the purpose of correlating the complex temporal classification results with their diverse features, we employed the Principal Component Analysis (PCA) (Maćkiewicz and Ratajczak, 1993) to reduce the dimensionality of the data. This method is commonly used in handling high-dimensional large datasets, as it can reduce data dimensionality, thereby enhancing data interpretability while minimizing information loss (Jolliffe and Cadima, 2016). Similarly, in this paper, we applied a similar approach to the high-dimensional temporal classification results, aiding us in analyzing the impact of various LULC features on prediction results.

3.4.1. Dynamic Time Warping (DTW)

In general, DTW is a method that calculates an optimal match between two given time series with certain restrictions and rules:

- Every index from the first sequence must be matched with one or more indices from the other sequence and vice versa.
- The first index from the first sequence must be matched with the first index from the other sequence (but it does not have to be its only match).
- The last index from the first sequence must be matched with the last index from the other sequence (but it does not have to be its only match).
- The mapping of the indices from the first sequence to indices from the other sequence must be monotonically increasing, and vice versa.

We can plot each match between the sequences $1 : M$ and $1 : N$ as a path in a $M \times N$ matrix from $(1, 1)$ to (M, N) , such that each step is one of $(1, 0), (0, 1), (1, 1)$. In this formulation, we see that the number of possible matches is the Delannoy number. The optimal match is the match that satisfies all the restrictions and the rules and that has the minimal cost, where the cost is computed as the sum of absolute differences for each matched pair of indices between their values. The sequences are ‘warped’ non-linearly in the time dimension to determine a measure of their similarity independent of certain non-linear variations in the time dimension. This sequence alignment method is often used in time series classification.

3.4.2. Principal Component Analysis (PCA)

PCA can be thought of as fitting a p-dimensional ellipsoid to the data, where each axis of the ellipsoid represents a principal component. For a column-wise zero empirical mean data matrix \mathbf{X} , the first component weight vector $w_{(1)}$

maximizes the data variance, so it must satisfies:

$$w_{(1)} = \arg \max_{\|w\|=1} \left\{ \sum_i (x_{(i)} \cdot w)^2 \right\} = \arg \max_w \left\{ \frac{w^\top \mathbf{X}^\top \mathbf{X} w}{w^\top w} \right\} \quad (12)$$

Other weight vectors can be obtained by continuing this progress after subtracting $\mathbf{X} w w^\top$ from \mathbf{X} . For example,

$$w_{(2)} = \arg \max_w \left\{ \frac{w^\top (\mathbf{X}_{(1)}^\top \mathbf{X}_{(1)}) w}{w^\top w} \right\}, \quad \text{where } \mathbf{X}_{(1)} = \mathbf{X} - \mathbf{X} w_{(1)} w_{(1)}^\top \quad (13)$$

where the component of \mathbf{X} on $w_{(i)}$ direction is the i th principle component of \mathbf{X} , which is called $p[i]$ in Figure 11.

4. Results

As indicated in Section 3, the weather data utilized in the experiments were sourced from weather stations and LULC data of the study area. To evaluate the performance of our model against existing microclimate prediction methods, we conducted a comparative study. When evaluating the model performance, considering that the target locations for prediction do not have weather stations, the historical weather data for the current prediction location is unavailable. To simulate such practical situations, it is crucial to avoid the direct inclusion of historical weather data for the target locations in the input dataset. Therefore, we adopted the commonly used method of cross-validation in machine learning: when predicting the weather data for each weather station, we excluded its own historical weather data and utilized only the historical weather data from other weather stations.

4.1. Evaluation Approach

In order to evaluate the model performance, the subsequent analysis of the results involves two types of baselines and commonly used error metrics. This section provides a detailed description of them.

4.1.1. Baselines

In existing studies, researchers often use urban weather files data or data from representative weather stations near the research target to access microclimate data for multiple types of studies. Therefore, to comprehensively validate the actual performance of the model proposed in this paper, we designed two levels of baselines. These baselines are compared with the experimental results of the model from the perspectives of machine learning algorithms and practical application scenarios. Our baselines consist of the following:

- Comparing the model with classical types of machine learning models to select the optimal algorithm that combines spatial and temporal data. The selected temporal baselines include LSTM and GRU, which are representative algorithms to process historical data; the selected spatial baselines include Ordinary Kriging and Regression Kriging interpolation. These are the level 1 baselines.
- Comparing the experimental results of the optimal ML algorithm with traditional microclimate data accessing methods, including directly using data from neighboring weather stations, representative urban weather stations (Weather station in Changi Airport), and International Weather for Energy Calculations (IWEC) data. The comparison could demonstrate the accuracy of our microclimate prediction method, also showing the practical implications. These are the level 2 baselines.

In order to conduct these studies, we compare the performance of the proposed Geo-LSTM-Kriging model.

4.1.2. Metrics

Mean Square Error (MSE), Rooted Mean Square Error (RMSE), and R^2 are computed as evaluation metrics. Equations (14) show the definition of these metrics. The error plotted in this paper is e_i in the equations.

O_i : observed values, S_i : simulated values $e_i = S_i - O_i$: error

$$\text{MSE} = \frac{1}{N} \sum_{i=1}^N (e_i)^2 = \frac{1}{N} \sum_{i=1}^N (O_i - S_i)^2$$

$$\text{RMSE} = \sqrt{\text{MSE}} = \sqrt{\frac{1}{N} \sum_{i=1}^N (O_i - S_i)^2}$$

$$R^2 = 1 - \frac{\sum_{i=1}^N (O_i - S_i)^2}{\sum_{i=1}^N (O_i - \bar{O})^2} \quad (14)$$

4.2. Baseline comparison

In this section, we will elaborate on the comparison between the model proposed in this paper and the two-level baselines mentioned in Section 4.1.1. We can discover the spatial and temporal trends of the local microclimate, as well as identify the environmental factors that influence the microclimate through the comparison of these experimental results.

4.2.1. Comparison with ML baselines

Due to the temporal nature of microclimates, in this paper, we conducted an hourly statistical analysis of the prediction results for all the weather stations, as shown in Figure 7. The horizontal axis represents the sequential time from 0 to 24 hours each day, while the vertical axis represents the absolute error between predicted values and actual values. The upper chart represents humidity, and the lower chart represents temperature. The box plots in the figure illustrate the trends of errors for each day and at each weather station location. The different colors represent the following different models: the Geo-LSTM-Kriging model, LSTM-Kriging model, GRU-Kriging model, Kriging model, and the IDW model respectively. It can be observed that for the humidity prediction results, we can see that traditional interpolation methods exhibit significant fluctuation in model prediction errors during the daytime from 11 a.m. to 6 p.m. In contrast, machine learning models reduce this error fluctuation, maintaining stable prediction errors throughout. However, both the LSTM-K and GRU-K machine learning models show a larger range of error fluctuations from around 0 a.m. to 8 a.m. Our GEO-LSTM-K model, on the other hand, maintains stable performance throughout the entire 24 hours. On the other hand, concerning the temperature prediction results, various methods show higher errors and greater variability during the daytime from 10 a.m. to 6 p.m.

For the fluctuation of prediction errors, it is evident that one reason is the significant variability in actual observational data during the corresponding time intervals, as depicted in Figure 3. The characteristics of these raw data naturally influence the prediction results, and a larger range of data fluctuations increases the difficulty of prediction, thus introducing greater variance in prediction errors. However, at the same time, we can observe that machine learning methods, especially the Geo-LSTM-Kriging model incorporating the Geo-layer, outperform traditional interpolation models significantly (RMSE of Geo-LSTM-Kriging reduces from 1.602 / 0.701 to 0.637 compared to IDW / LSTM-Kriging respectively, shown in Table 3). This indicates that machine learning, along with the introduction of the Geo-layer, contributes to the model capturing new knowledge. This kind of fluctuation is reasonable in urban meteorology, as various factors such as local natural conditions such as solar radiation, shading, rainfall, the surrounding built environment related to the UHI effect, urban heat exchange, and more contribute to increased instability in microclimate data during the day.

To further analyze the optimization effect and explore the knowledge acquired by the models through the Geo-layer, we summarize the variance and fluctuation range of the prediction errors of these two models in Figure 8. This figure contrasts the Geo-LSTM-Kriging and LSTM-Kriging models extracted separately from the previous figure. Differing from Figure 3, the blue numbers in this figure represent the standard deviation of the prediction errors for the Geo-LSTM-Kriging model during each hour, while the orange numbers represent the standard deviation for the LSTM-Kriging model. Upon closer inspection, it can be observed that during periods of significant fluctuations in the original data, particularly during periods of early morning humidity and afternoon temperature (as shown in Figure 3), the addition of the Geo-layer results in more stable predictions, with a noticeably larger reduction in variance. For example, the standard deviation of temperature prediction errors decreased from 0.96 to 0.57 at 13:00 in the afternoon, while it only decreased from 0.67 to 0.41 at 23:00 at night. The overall statistical results (RMSE) and R^2 will be summarized after comparing with the level-2 baselines, as shown in Table 3.

This suggests that the Geo-layer, to some extent, has learned the varying impact of environmental factors such as UHI on temperature and humidity during different time periods. Our model aims to uncover the underlying reasons for how geographical environmental factors influence the performance of meteorological data, providing more stable predictive results. In the above figure, we have depicted the model prediction errors at all weather station locations in boxes. Apart from time series analysis, different LULC features among various weather stations can also have varying

effects on prediction performance. Detailed analysis of how these LULC features specifically affect model performance will be presented in the subsequent spatial analysis, after the comparison with level-2 baselines.

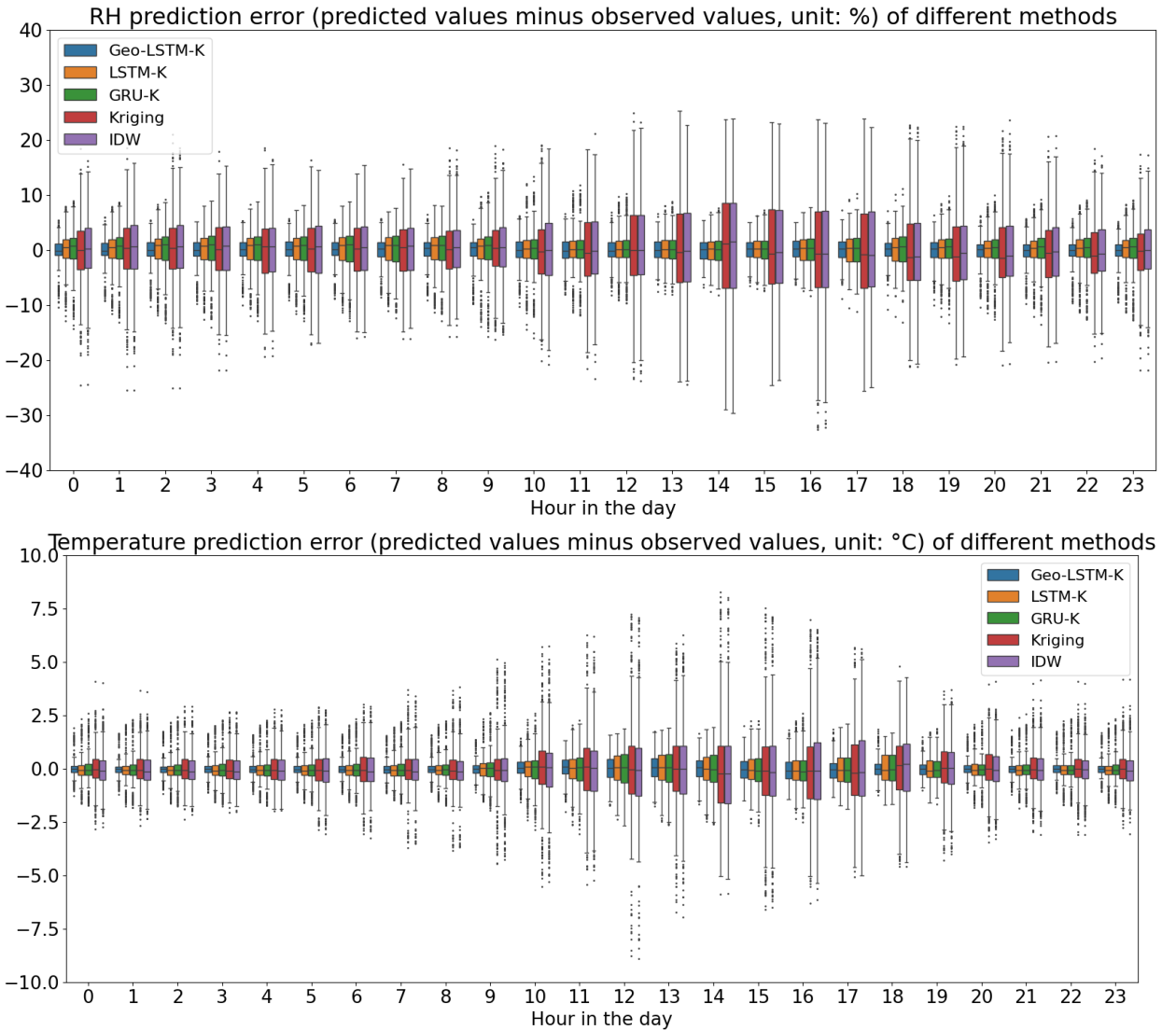


Figure 7: Temporal comparison between LSTM-Kriging and ML (level 1) baselines.

4.2.2. Comparison with practical baselines

In practical applications, as mentioned in Section 4.1, many studies often directly use weather file data or data from representative urban weather stations when requiring microclimate data. Therefore, in this section, we compare the prediction results with several commonly used data acquisition methods, marked as different colors in Figure 9. In the various models mentioned below, we assume that the target location for prediction does not have any weather station with measured data. Instead, we perform interpolation prediction using data from the other 13 weather stations. Subsequently, we compare the predicted results with the actual ground truth at the target point to obtain the corresponding error. The error at each hour is the aggregated distribution of errors at all the 14 weather stations' locations. The orange one represents the method of using data from the nearest meteorological station to the target location, which is a commonly used approach in microclimate-related studies. The green one represents the use of

Microclimate spatio-temporal prediction

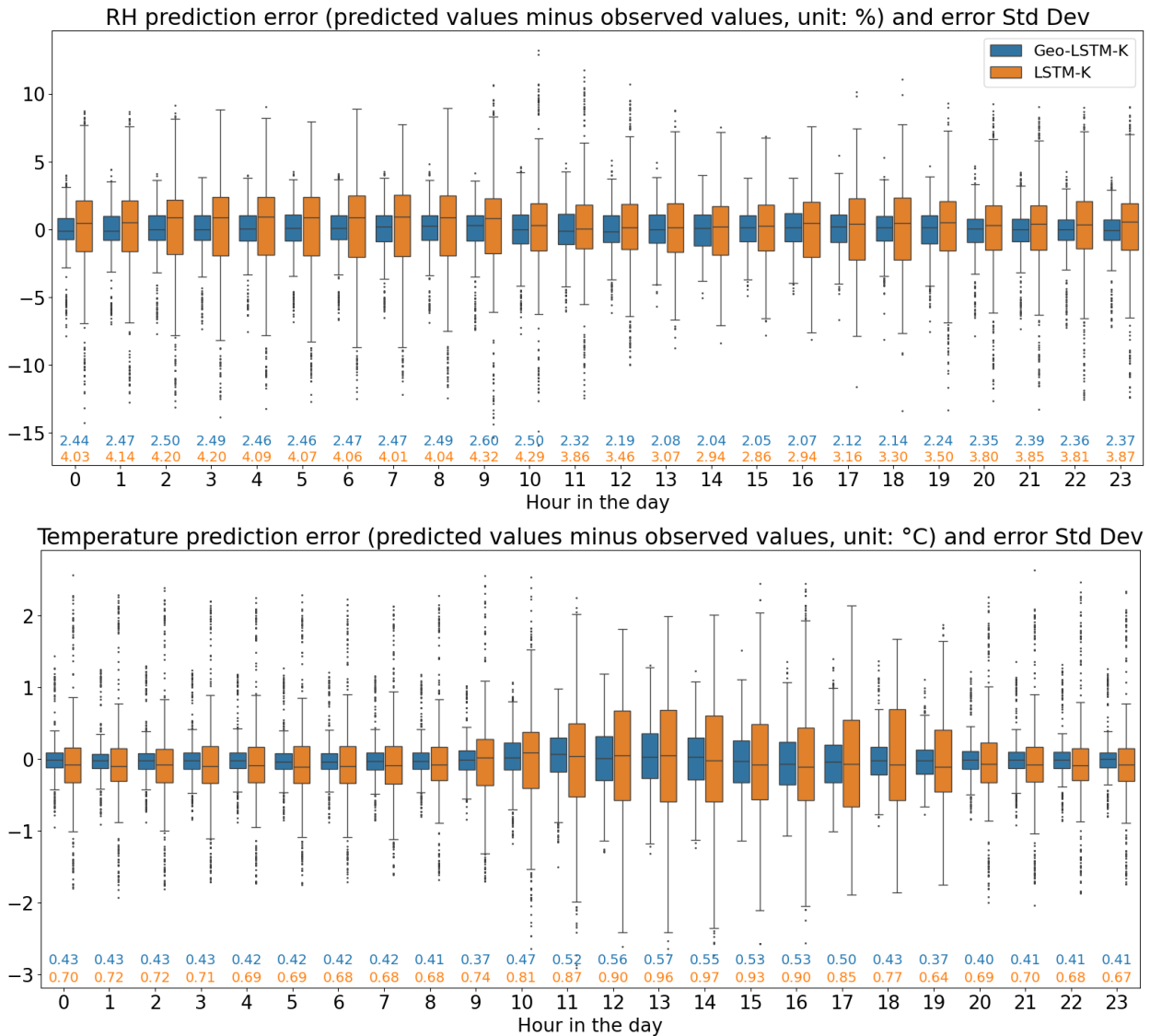


Figure 8: Temporal comparison between Geo-LSTM-Kriging and LSTM-Kriging.

local International Weather for Energy Calculations (IWEC) data in Singapore, obtained on EnergyPlus, which is a standard weather file commonly used directly in energy simulations. The red one represents the weather data measured by the weather station at Changi Airport in Singapore.

From the above figure, we can observe several intriguing phenomena. The most evident difference lies in the higher humidity and lower temperature observed in the IWEC data compared to the local NUS campus data. We can reasonably speculate that this discrepancy is related to the historical lag in IWEC data. With the intensification of the greenhouse effect, the global warming phenomenon has become increasingly pronounced in recent years. Clearly, conventional meteorological data has become outdated. In studies utilizing typical weather files, researchers should be attentive to this aspect. Existing research indicates that updated typical weather files, compared to outdated ones, can have a significant impact of up to 50–65% on building energy simulations. (Costanzo, Evola, Infantone and Marletta, 2020), the issue of weather file outdatedness has become increasingly imperative in studies pertaining to microclimate. On the other hand, a stark contrast in the deviation patterns is discernible when comparing the data from Changi Airport with that of the NUS campus. Changi Airport exhibits a conspicuous disparity, with consistently lower average humidity

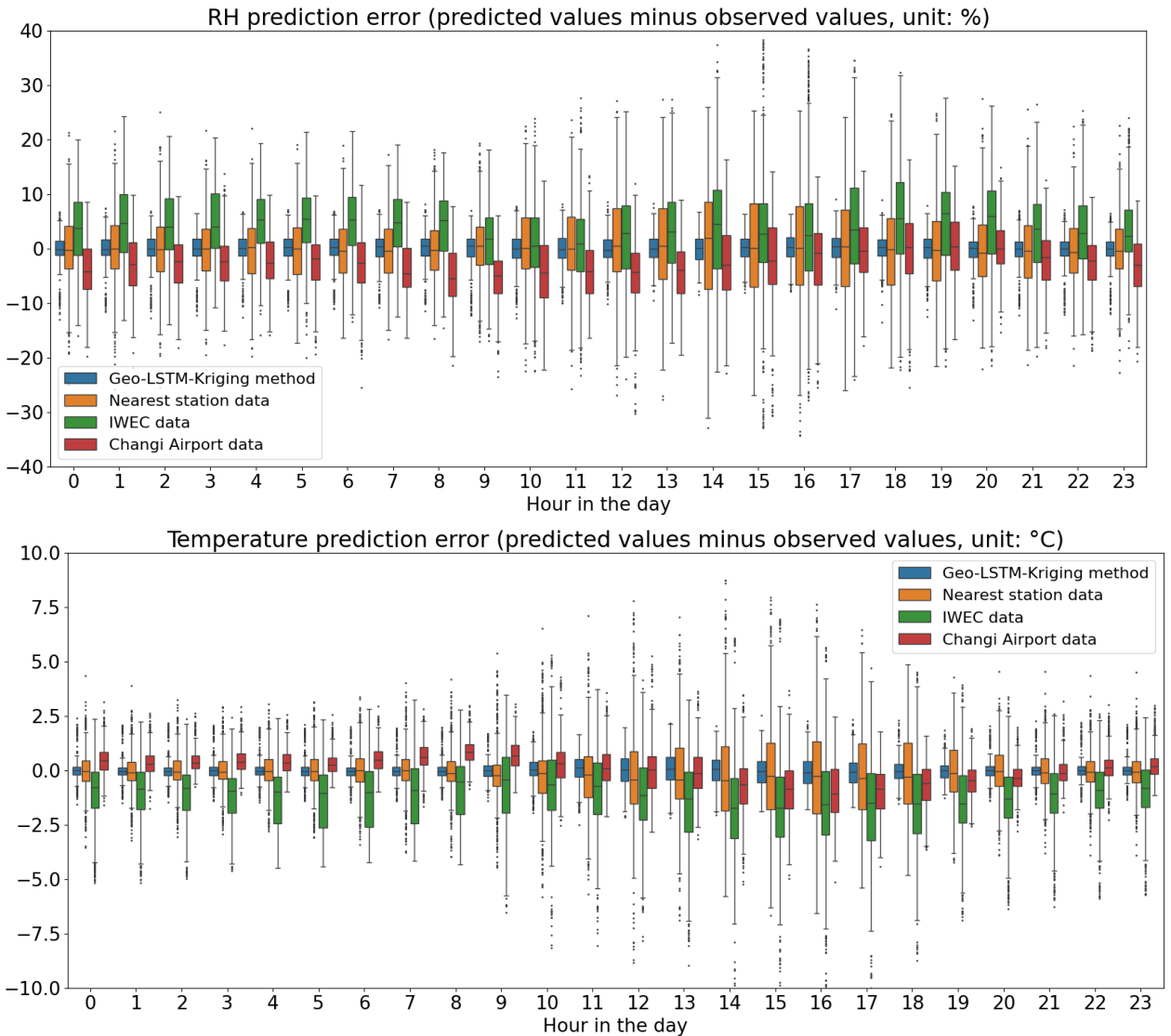


Figure 9: Temporal comparison between Geo-LSTM-Kriging and practical (level-2) baselines.

and higher temperatures. It is noteworthy that temporal consistency between the two datasets was ensured during the plotting process. Therefore, a reasonable inference can be made that such data discrepancies stem from divergent local environmental conditions. In comparison to the open and flat geographical environment of the airport, the NUS campus boasts a higher vegetation coverage. Such geographical conditions have the potential to mitigate issues such as the UHI effect, thereby reducing surface temperatures. In order to rigorously investigate the influence of various features within the Land Use and Land Cover (LULC) data on the environment and model performance, we will conduct spatial analysis on 14 weather stations in the subsequent section, providing a more quantified theoretical basis.

Additionally, as mentioned in the preceding section, we summarized the overall comparative results of our model and the two-level baseline in Table 3. The RMSE and variance in the table represent the overall performance across all 14 weather stations for the entire month. Upon observing the table, it is evident that machine learning models exhibit a significant improvement compared to conventional interpolation models (e.g., the RMSE for temperature decreased from 1.59 in Kriging to 0.70 in LSTM-Kriging, and the R^2 for RH increased from 0.673 in Kriging to 0.931 in LSTM-Kriging). We selected a machine learning model with outstanding performance and introduced a Geo-layer.

With the addition of the Geo-layer, there was an improvement in the RMSE for temperature, decreasing from 0.70 to 0.64, while other indicators showed less pronounced changes. Among the level-2 baselines, the data from Changi Airport performed relatively better but still exhibited a noticeable gap compared to the LSTM-Kriging model. The specific performance of the model at different weather stations and its correlation with their respective LULC features will be detailed in the next section on spatial analysis.

Table 3
RMSE and R² of the prediction error of different methods.

	Geo-LSTM-K	Level 1 baselines				Level 2 baselines		
		LSTM-K	GRU-K	Kriging	IDW	Nearest	IWEC	Changi Airport
RMSE (Temp.)/°C	0.64	0.70	0.70	1.60	1.60	1.72	2.37	1.09
RMSE (RH) /%	3.23	3.43	3.44	7.70	7.74	8.19	9.50	6.73
R ² (Temp.)	0.9975	0.9950	0.9945	0.9850	0.9848	0.9640	0.9823	0.9930
R ² (RH)	0.9385	0.9309	0.9306	0.6727	0.6752	0.6362	0.6106	0.6899

4.3. Model spatial performance analysis

After analyzing the temporal aspects of the prediction results, we proceeded with a comprehensive spatial analysis based on the different geographical conditions. We calculated the prediction errors for all 14 stations and found that their trends over time vary among different weather stations. Therefore, we categorized these weather stations according to the temporal prediction error at their spatial locations' performance including both temperature and RH prediction errors. Such classification results are further analyzed combined with their LULC features, to explore the potential pattern of the environmental effects.

In the actual classification process, we treated the prediction errors of temperature and humidity for each hour of every day within a month at each weather station as a time series data point. We aggregated these data points and performed clustering. Specifically, for instance, if, among the 30 data points for Weather Station 1, 20 belong to cluster 0 and 10 belong to category 1, then we conclude that Weather Station 1 has 1/3 of its attributes belonging to category 1 and 2/3 belonging to category 0 (this is a simplified example for illustration purposes and is not related to actual results). Figure 10 illustrates the clustering results obtained using the DTW algorithm, as mentioned in Section 3.4.1. Different colors represent the temporal performance of prediction errors for different clusters of weather stations. The left panel represents humidity prediction errors, while the right panel represents temperature prediction errors. It is noteworthy that only Weather Station 8 is in cluster 0, and it exhibits higher errors in all the models, including baselines, compared to other weather stations. In Figure 2, a comparison is made between the actual measurements of Weather Station 8 and those of other weather stations. It is evident that the actual data for Weather Station 8 significantly differs from the data of other weather stations across the campus. Its temperature is consistently lower throughout the 24 hours, and the humidity is higher. Hence, the higher prediction errors when using other weather stations for interpolation can be explained.

Figure 12 shows the overall classification results, where PCA was employed to reduce data dimensionality, transforming the 24-dimensional time series data into two dimensions (x and y) for better observation of the clustering results. Here, we observe that cluster 0 (depicted in blue), representing Weather Station 8, is distant from the other weather stations, while the other three clusters exhibit certain degrees of cohesion, which indicates the classification results are deemed reasonable.

Upon closer examination of Figure 10, it becomes evident that, apart from the isolated Weather Station 8, the other three categories of weather stations also exhibit distinct trends in prediction errors. In cluster 1 (depicted in orange), the prediction error for RH is lower during the midday period (10:00-14:00), while the prediction error for temperature is higher during this interval. Cluster 2 (depicted in green) demonstrates relatively stable prediction errors throughout the entire period. Conversely, cluster 3 (depicted in red) exhibits trends opposite to those in cluster 1. To delve deeper into the correlation between prediction errors across different clusters and the corresponding LULC features of various weather stations, we further employed PCA to reduce data dimensionality and generated Figure 13. In this figure, the x-axis represents the values of the principal components obtained through PCA for the reduced dimensionality of time series prediction errors at all the weather stations, while the y-axis in each subfigure represents the values

of different LULC features. In general, the relationship between prediction errors and LULC features is intricate, making simple correlation assessments unfeasible. However, certain features manifest more pronounced influences in specific instances. In Table 4, we summarize several features that exhibit differences in performance among weather stations in different clusters. We can observe differences in these features among different categories (excluding the standalone cluster 0). The varying distances to buildings and walkways imply differences in shading conditions at different times of the day. For instance, Cluster 1 has an average distance to buildings of approximately 9.7 meters, while Cluster 3 has an average distance of about 23.09 meters. This suggests that buildings may provide more shading for Cluster 1, causing weather stations in Cluster 1 to exhibit larger fluctuations during the noon period. The observed discrepancies between the model predictions and the actual conditions, with lower humidity and higher temperature in our predictions, might be attributed to the incomplete learning of the impact of building shadows. However, due to the limited number of weather stations, a more systematic quantitative analysis is not feasible and we can only provide a qualitative and reasonable inference. We can infer that these features likely have varying degrees of influence on predictions for different weather stations and different time periods.

Due to the limited number of weather stations in this study, there are notable constraints on the correlation analysis between clustering results and LULC features. Nevertheless, within the restricted dataset of 14 weather stations, we have identified certain patterns, indicating that different LULC features exert varying degrees of influence on model performance. These features provide distinct environmental conditions for the target locations, leading to diverse manifestations of urban heat island effects, urban heat exchange, urban surface characteristics, and other related factors. Consequently, these impacts are reflected in the model prediction performances, resulting in diverse levels of errors and stability. The associated effects merit further investigation in future studies involving a more extensive array of weather stations.

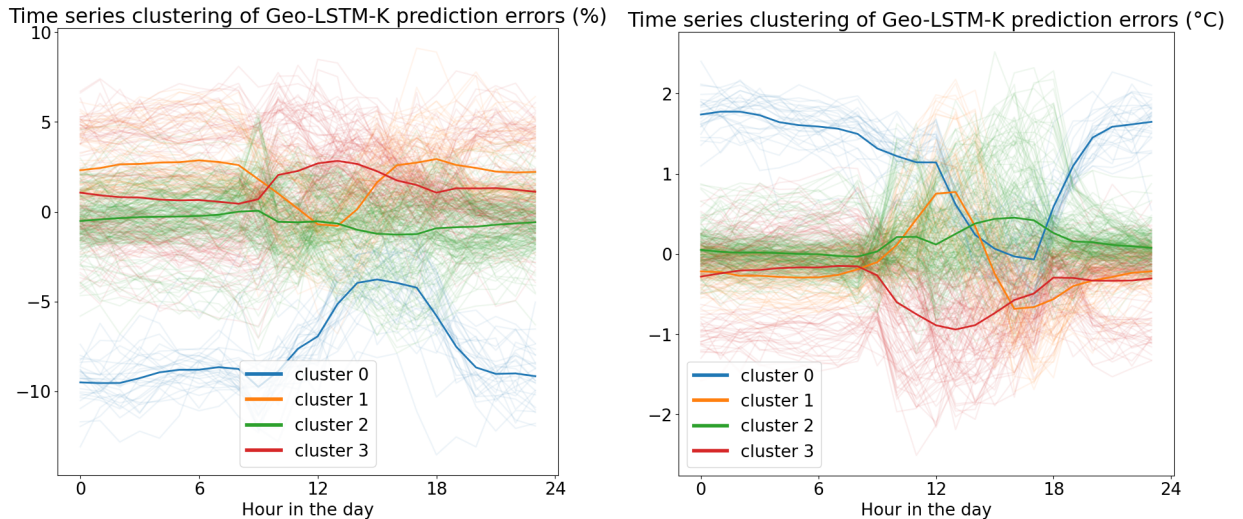


Figure 10: Clustering of weather stations based on the prediction errors.

Table 4
LULC feature data.

Cluster id	0	1	2	3
Terrain Std Dev	10.4	10.6	8.9	7.5
Terrain mean	35.1	30.9	38.2	25.4
DistToBuilding Std Dev	6.5	6.7	7.7	11.9
DistToBuilding mean	9.08	9.70	5.94	23.09
DistToWalkway Std Dev	81.74	69.00	161.40	87.85
DistToWalkway mean	173.96	130.48	194.34	145.03

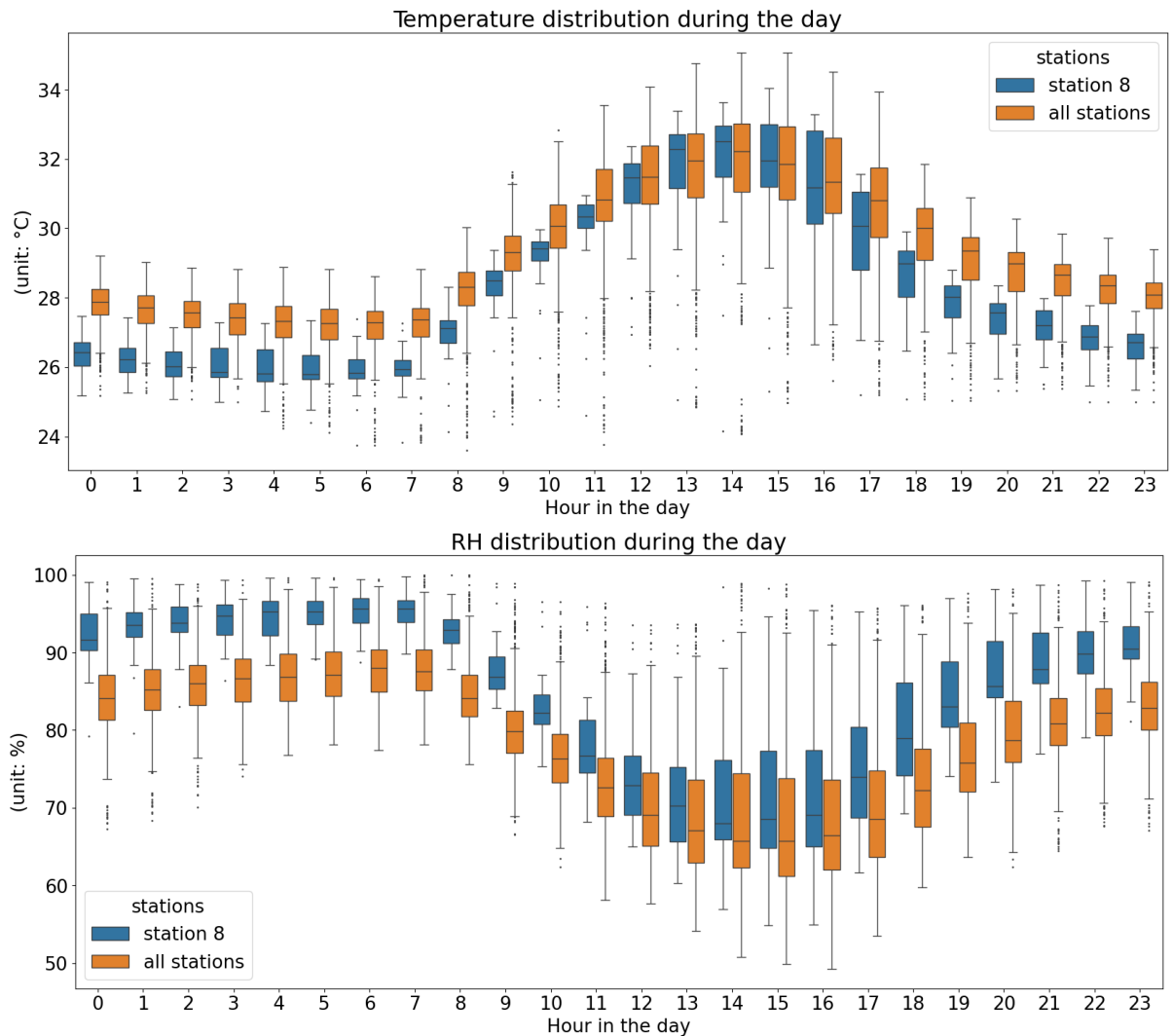


Figure 11: Comparison of the temperature data of station 8 with all the other stations

5. Discussion

In this section, we will provide a typical application scenario for the model and some general model performance discussions.

A commonly used application scenario is to provide high-precision, high-resolution visualized prediction results for the impact of changes in building and environmental conditions on microclimates within a small area. For instance, Figure 14 displays the model predictions for humidity and temperature at three different time points, from top to bottom: the predictions for 04:00 on July 5th, 20:00 on July 9th, and 12:00 on July 22nd. Our model initially learns geographical information through the Geo-Kriging layer. Subsequently, the model downscale the historical data from the original weather stations to a finer grid. After that, the LSTM layer is employed to predict and generate this map based on the downscaled data. In this figure, we did not depict any actual buildings or road objects, but the high-density predictions at different time intervals partially reflect the outlines of roads and buildings, especially noticeable during the midday period, where the temperature predictions essentially outline the distribution of roads within the area. In the ever-changing built environment, such as when urban planners are considering increasing vegetation coverage in a specific area or when certain buildings require renovation, expansion, or demolition, this model can proactively offer detailed temporal results of microclimate data, providing valuable insights for related decision-making.

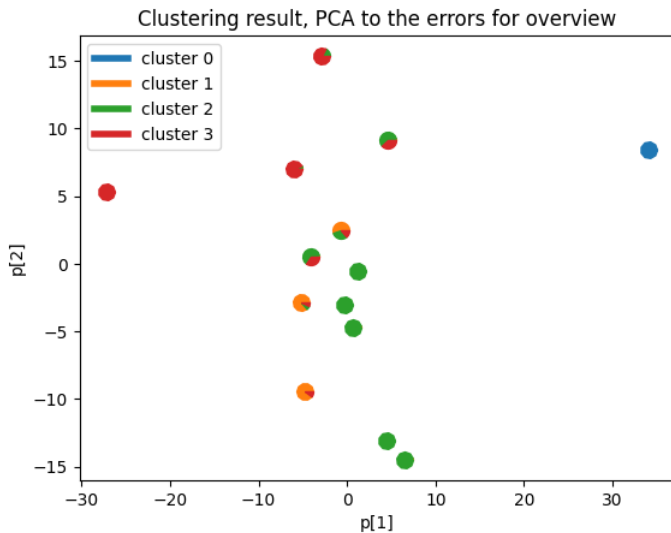


Figure 12: Station clustering result based on DTW analysis over the error series at each station location.

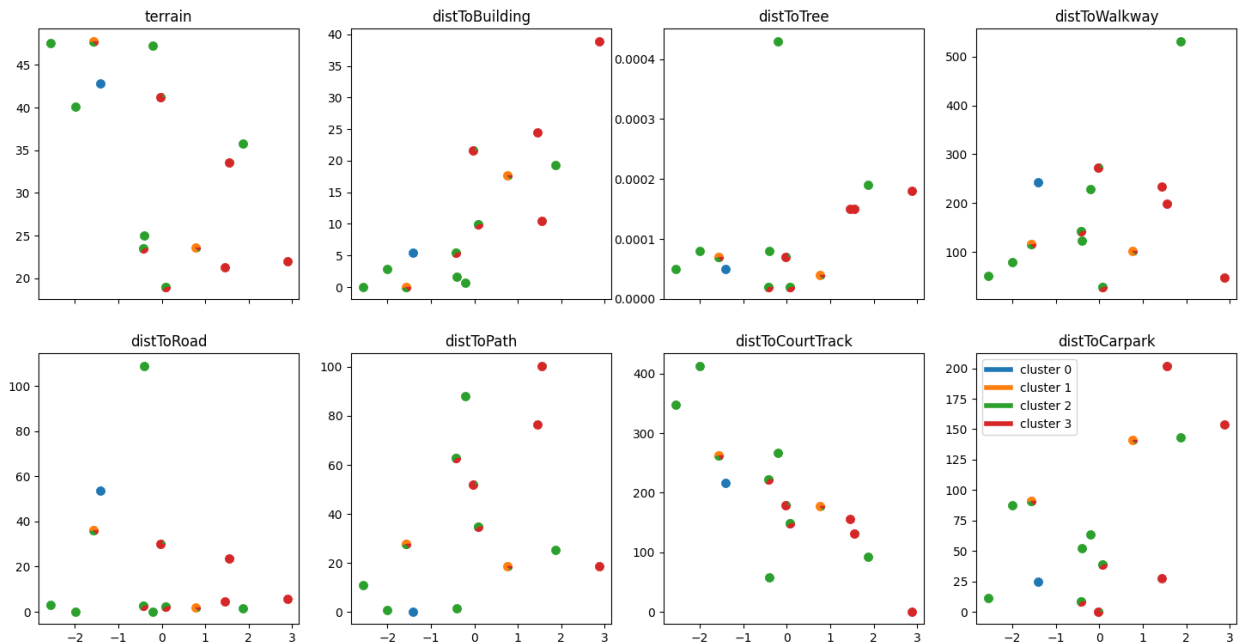


Figure 13: The distribution of LULC features and PCA values of stations in each cluster.

In addition to the discussed applications, our predictions of microclimates can assist various research problems. Besides the traditional studies mentioned in the related work section, such as high-precision BPS, thermal comfort, residents' health, and building material lifespan, the predictions in high-spatial and high-temporal dimensions can aid in establishing urban or district digital twins. Namely, these predictions provide real-time and high-resolution input to support digital twins, enabling simulations and achieving a feedback loop with the real-world, which is currently often missing (Lei, Janssen, Stoter and Biljecki, 2023; Liu, Zhao, Luo, Lei, Frei, Miller and Biljecki, 2023).

Microclimate spatio-temporal prediction

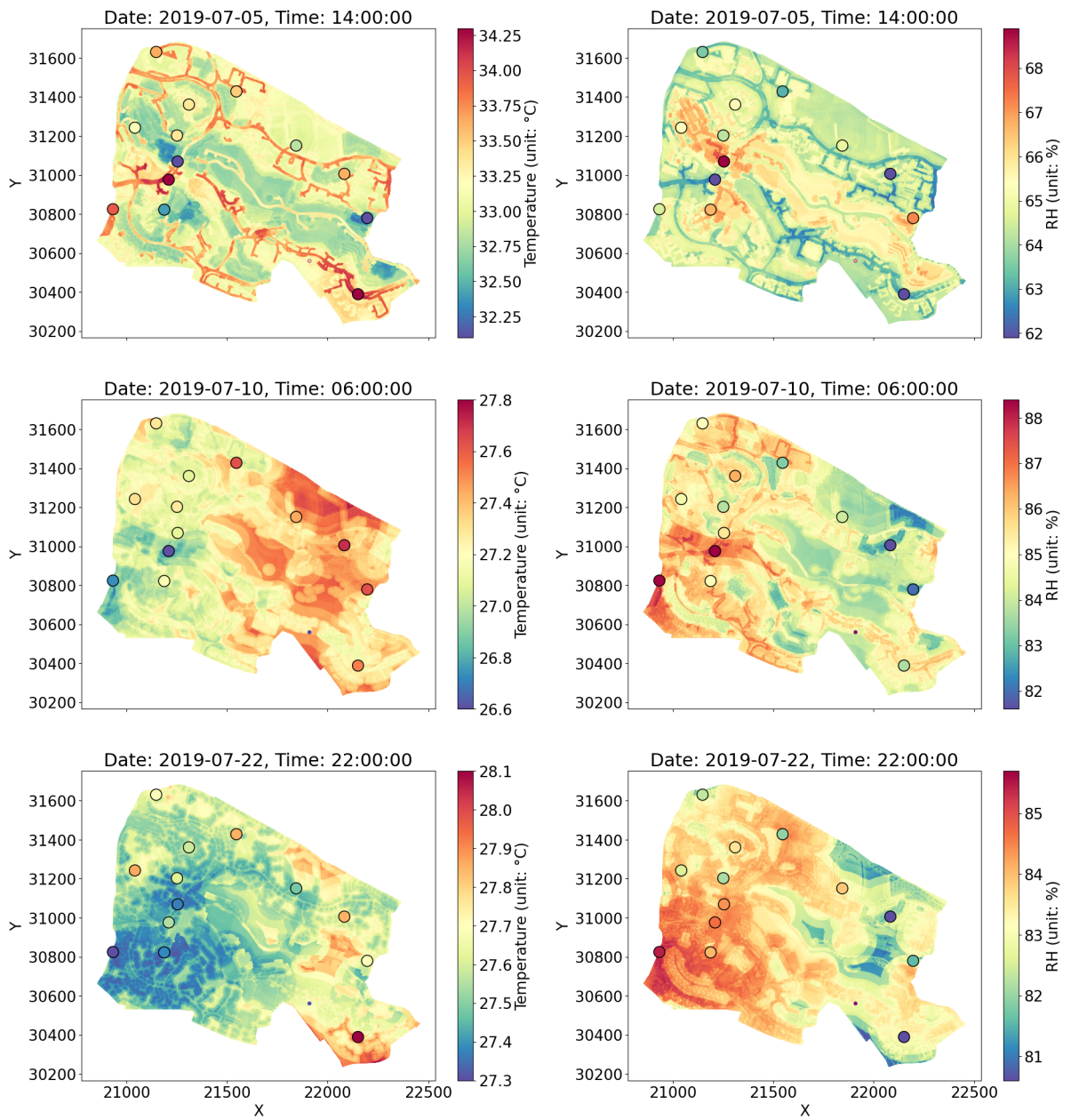


Figure 14: Prediction result samples of Geo-LSTM-Kriging model. The units in the maps are in metres (based on the local coordinate system SVY21), while the legend units for Temperature and RH are in °C and %, respectively.

This study proposes a novel microclimate prediction model, the LSTM-Kriging model, which combines both temporal and spatial knowledge. Furthermore, this model incorporates LULC through the Geo-LSTM-Kriging model to adapt to the influences of urban environmental obstacles. Our experiment results demonstrate the effectiveness of this methodology in a range of actual cases, particularly in moments with dramatic environmental changes.

Compared to past research, the model proposed in this paper has several innovative aspects. Firstly, our predictions achieve a spatial resolution of 1 meter grid, whereas Di Napoli et al. (2020) using NWP to obtain prediction results with a spatial resolution of 2.5 x 2.5 km, Chang et al. (2021) developing a UMTF model to predict the microclimate with a spatial resolution of 50 x 50 m. This significant improvement in spatial resolution holds considerable importance for studies that require higher microclimate spatial density. Besides, our approach provides a fresh perspective on

weather prediction models, particularly in scenarios with environmental variations. Erell and Zhou (2022) indicated that achieving a green surface proportion of 0.5 would result in a decrease of approximately 0.3 °C in the annual average temperature. Our analysis of the impact of LULC data shows that considering LULC data reduces the MAE from 0.61 °C to 0.12 °C, thereby further confirming the significance of considering environmental conditions on microclimate. Our model's capacity to adapt to urban environmental obstacles renders it a valuable tool for weather prediction in urban environments. Additionally, traditional research often relies on directly using data from neighboring weather stations or classic weather files (Krüger, Drach, Emmanuel and Corbella, 2013; Kruger and Drach, 2017; Li and Liu, 2020), which can be insufficiently accurate in certain microclimate studies. The model proposed in this study offers temperature and humidity predictions for microclimates with spatial resolution and achieves better performance compared with weather stations and weather files. At the same time, the data required for this method is widely and freely available at a sufficient level of quality, e.g. from volunteered geographic information platforms such as OpenStreetMap (Biljecki, Chow and Lee, 2023a; Herfort, Lautenbach, Albuquerque, Anderson and Zipf, 2023), allowing wide applicability.

6. Conclusion

This study proposes the LSTM-Kriging model, which combines both temporal and spatial knowledge to develop a novel weather interpolation model, enabling the prediction of microclimate conditions at high resolution in the built environment. Our Geo-LSTM-Kriging model further incorporates LULC data to adapt to the influences of urban environmental obstacles. Our experiment results demonstrate the effectiveness of this methodology in a range of actual cases, particularly in moments with dramatic environmental fluctuations.

The study introduces several key findings:

- Our approach provides an improvement over traditional microclimate prediction baselines, demonstrating the importance of incorporating spatial, temporal, and geographical knowledge (LULC) in the model. Compared to the direct use of urban weather station (Changi Airport) data, the temperature prediction RMSE of our high spatial-resolution model has reduced from 1.09 °C to 0.64 °C, the RH prediction RMSE has decreased from 6.73 to 3.23. While the traditional interpolation method (Kriging interpolation) yielded a temperature prediction RMSE of 1.59 °C and an RH RMSE of 7.70. The addition of the Geo-layer helped reduce the prediction error of temperature from 0.70 °C to 0.64 °C and of humidity from 3.43 to 3.23.
- The analysis in the paper regarding the influence of different LULC data from various weather stations on the prediction results indicates that the extent of building and vegetation coverage in the environment can lead to varying degrees of impact on microclimate prediction during different time periods. The addition of Geo-layer allows for learning the impact of LULC features to some extent, enhancing the stability of the model predictions, especially during periods of significant fluctuations in the original data. For instance, the standard deviation of the temperature prediction error at 13:00 reduced from 0.96 to 0.57.
- This study also conducted a temporal analysis of model errors for weather station clustering. It was observed that among various LULC features, terrain, distance to buildings, and distance to walkways might have a greater influence on the model performance.

However, the study also identified some limitations and a few open questions remain unanswered. Our experiments implemented for the Geo-LSTM-Kriging model are restricted to a small area with only 14 weather stations, and hence, the analysis and conclusions drawn from the clustering results are highly limited. Furthermore, the model does not consider the effect of vertical dimension, which may not be a negligible factor when considering geographical information. Additionally, there are some typical features that are also crucial for microclimate research, such as wind speed, solar radiation, etc. This paper primarily focuses on discussing temperature and RH, with the expansion to other features expected to be explored in future research. Despite these limitations, due to notable advancements in performance, we believe that our study provides a contribution to the field of weather forecasting in urban environments, which could be further improved and applied to specific tasks.

Future research should focus on expanding the model's applicability to other geographical locations and scaling it to larger areas, and incorporating more comprehensive data, such as classified point cloud data and street-level imagery, which may add further value to the predictions thanks to their high resolution and additional information (Megahed, Shaker and Yan, 2021; Biljecki, Zhao, Liang and Hou, 2023b). Moreover, the form of the employment of geographical

information could be explored beyond the convolution-like layer structure proposed in this study. With these improvements, the proposed model could be a valuable tool for weather forecasting and urban planning.

Data availability

The research compendium for this article can be found at:

<https://github.com/ideas-lab-nus/microclimate-dl-predict>

Acknowledgements

This research project is supported by the Singapore Ministry of Education Academic Research Fund (MOE-ARF) Tier 1 (grant number A-8000139-00-00); the National Research Foundation, Singapore, and Ministry of National Development, Singapore under its Cities of Tomorrow R&D Programme (CoT Award COT-V4-2020-5). We thank Dr. Marcel Ignatius for his initial input and support in the early stages of this study.

CRediT authorship contribution statement

Han Jintong: Methodology, Software, Formal analysis, Investigation, Visualization, Writing - Original Draft. **Adrian Chong:** Conceptualization, Methodology, Supervision, Writing - Review & Editing, Funding acquisition. **Joie Lim:** Resources, Data Curation. **Savitha Ramasamy:** Conceptualization, Methodology, Writing - Review & Editing. **Wong Nyuk Hien:** Resources. **Filip Biljecki:** Visualization, Writing - Review & Editing, Project administration, Funding acquisition.

References

- Abanda, A., Mori, U., Lozano, J.A., 2019. A review on distance based time series classification. *Data Mining and Knowledge Discovery* 33, 378–412.
- Abdullah, S., Barua, D., Abdullah, S.M.A., Rabby, Y.W., 2022. Investigating the impact of land use/land cover change on present and future land surface temperature (lst) of chittagong, bangladesh. *Earth Systems and Environment* 6, 221–235.
- Aggarwal, R., Kumar, R., 2013. A comprehensive review of numerical weather prediction models. *International Journal of Computer Applications* 74.
- Agterberg, F.P., 1984. Trend surface analysis, in: Spatial statistics and models. Springer, pp. 147–171.
- Akbari, H., Cartalis, C., Kolokotsa, D., Muscio, A., Pisello, A.L., Rossi, F., Santamouris, M., Synnefa, A., Wong, N.H., Zinzi, M., 2016. Local climate change and urban heat island mitigation techniques—the state of the art. *Journal of Civil Engineering and Management* 22, 1–16.
- Aliabadi, A.A., McLeod, R.M., 2023. The vatic weather file generator (vwfg v1. 0.0). *Journal of Building Engineering* 67, 105966.
- Alimukhamedov, D., et al., 2022. Hygienic analysis of microclimate parameters influence on workers' health in plants manufacturing polymer products, in: 2022, pp. 128–130.
- Arnfield, A.J., 2003. Two decades of urban climate research: a review of turbulence, exchanges of energy and water, and the urban heat island. *International Journal of Climatology: a Journal of the Royal Meteorological Society* 23, 1–26.
- Azawi, H., Saleh, M.S., 2021. Review of the kriging technique applications to groundwater quality. *Journal of Engineering* 27, 23–32.
- Bamdad, K., Cholette, M.E., Omrani, S., Bell, J., 2021. Future energy-optimised buildings—addressing the impact of climate change on buildings. *Energy and Buildings* 231, 110610.
- Bartier, P.M., Keller, C.P., 1996. Multivariate interpolation to incorporate thematic surface data using inverse distance weighting (idw). *Computers & Geosciences* 22, 795–799.
- Bevilacqua, P., Morabito, A., Bruno, R., Ferraro, V., Arcuri, N., 2020. Seasonal performances of photovoltaic cooling systems in different weather conditions. *Journal of Cleaner Production* 272, 122459.
- Bijarniya, J.P., Sarkar, J., Maiti, P., 2020. Environmental effect on the performance of passive daytime photonic radiative cooling and building energy-saving potential. *Journal of Cleaner Production* 274, 123119.
- Bile, A., Tari, H., Grinde, A., Frasca, F., Siani, A.M., Fazio, E., 2022. Novel model based on artificial neural networks to predict short-term temperature evolution in museum environment. *Sensors* 22, 615.
- Biljecki, F., Chow, Y.S., Lee, K., 2023a. Quality of crowdsourced geospatial building information: A global assessment of OpenStreetMap attributes. *Building and Environment* 237, 110295. doi:10.1016/j.buildenv.2023.110295.
- Biljecki, F., Zhao, T., Liang, X., Hou, Y., 2023b. Sensitivity of measuring the urban form and greenery using street-level imagery: A comparative study of approaches and visual perspectives. *International Journal of Applied Earth Observation and Geoinformation* 122, 103385. doi:10.1016/j.jag.2023.103385.
- Caballero, C.B., Ruhoff, A., Biggs, T., 2022. Land use and land cover changes and their impacts on surface-atmosphere interactions in brazil: A systematic review. *Science of The Total Environment* 808, 152134.
- Chakraborty, T., Sarangi, C., Lee, X., 2021. Reduction in human activity can enhance the urban heat island: Insights from the covid-19 lockdown. *Environmental Research Letters* 16, 054060.

Microclimate spatio-temporal prediction

- Chang, J.M.H., Lam, Y.F., Lau, S.P.W., Wong, W.K., 2021. Development of fine-scale spatiotemporal temperature forecast model with urban climatology and geomorphometry in hong kong. *Urban Climate* 37, 100816.
- Costanzo, V., Evola, G., Infantone, M., Marletta, L., 2020. Updated typical weather years for the energy simulation of buildings in mediterranean climate. a case study for sicily. *Energies* 13, 4115.
- Crank, P.J., Sailor, D.J., Ban-Weiss, G., Taleghani, M., 2018. Evaluating the envi-met microscale model for suitability in analysis of targeted urban heat mitigation strategies. *Urban climate* 26, 188–197.
- Deilami, K., Kamruzzaman, M., Liu, Y., 2018. Urban heat island effect: A systematic review of spatio-temporal factors, data, methods, and mitigation measures. *International journal of applied earth observation and geoinformation* 67, 30–42.
- Di Napoli, C., Hogan, R.J., Pappenberger, F., 2020. Mean radiant temperature from global-scale numerical weather prediction models. *International Journal of Biometeorology* 64, 1233–1245.
- Erell, E., Zhou, B., 2022. The effect of increasing surface cover vegetation on urban microclimate and energy demand for building heating and cooling. *Building and Environment* 213, 108867.
- Estoque, R.C., Murayama, Y., Myint, S.W., 2017. Effects of landscape composition and pattern on land surface temperature: An urban heat island study in the megacities of southeast asia. *Science of the Total Environment* 577, 349–359.
- Gaur, S., Singh, R., 2023. A comprehensive review on land use/land cover (lulc) change modeling for urban development: current status and future prospects. *Sustainability* 15, 903.
- Gia Pham, T., Kappas, M., Van Huynh, C., Hoang Khanh Nguyen, L., 2019. Application of ordinary kriging and regression kriging method for soil properties mapping in hilly region of central vietnam. *ISPRS International Journal of Geo-Information* 8, 147.
- Granville, K., Woolford, D.G., Dean, C., Boychuk, D., McFayden, C.B., 2023. On the selection of an interpolation method with an application to the fire weather index in ontario, canada. *Environmetrics* 34, e2758.
- Han, J.M., Ang, Y.Q., Malkawi, A., Samuelson, H.W., 2021. Using recurrent neural networks for localized weather prediction with combined use of public airport data and on-site measurements. *Building and Environment* 192, 107601.
- Hayles, C., Huddleston, M., Chinowsky, P., Helman, J., 2022. Quantifying the effects of projected climate change on the durability and service life of housing in wales, uk. *Buildings* 12, 184.
- Heidari, H., Mohammadbeigi, A., Khazaei, S., Soltanzadeh, A., Asgarian, A., Saghabipour, A., 2020. The effects of climatic and environmental factors on heat-related illnesses: A systematic review from 2000 to 2020. *Urban Climate* 34, 100720.
- Herfort, B., Lautenbach, S., Albuquerque, J.P.d., Anderson, J., Zipf, A., 2023. A spatio-temporal analysis investigating completeness and inequalities of global urban building data in OpenStreetMap. *Nature Communications* 14, 3985. doi:10.1038/s41467-023-39698-6.
- Hochreiter, S., Schmidhuber, J., 1997. Long short-term memory. *Neural computation* 9, 1735–1780.
- Hosseini, M., Lee, B., Vakilinia, S., 2017. Energy performance of cool roofs under the impact of actual weather data. *Energy and Buildings* 145, 284–292.
- Hütt, C., Koppe, W., Miao, Y., Bareth, G., 2016. Best accuracy land use/land cover (lulc) classification to derive crop types using multitemporal, multisensor, and multi-polarization sar satellite images. *Remote sensing* 8, 684.
- Im, H., Srinivasan, R.S., Maxwell, D., Steiner, R.L., Karmakar, S., 2022. The impact of climate change on a university campus' energy use: Use of machine learning and building characteristics. *Buildings* 12, 108.
- Imanian, H., Shirkhani, H., Mohammadian, A., Hiedra Cobo, J., Payeur, P., 2023. Spatial interpolation of soil temperature and water content in the land-water interface using artificial intelligence. *Water* 15, 473.
- Jolliffe, I.T., Cadima, J., 2016. Principal component analysis: a review and recent developments. *Philosophical transactions of the royal society A: Mathematical, Physical and Engineering Sciences* 374, 20150202.
- Kartal, S., 2022. Prediction of modis land surface temperature using new hybrid models based on spatial interpolation techniques and deep learning models. *Environmental Science and Pollution Research*.
- Koc, M., Acar, A., 2021. Investigation of urban climates and built environment relations by using machine learning. *Urban Climate* 37, 100820.
- Krüger, E., Drach, P., Emmanuel, R., Corbella, O., 2013. Assessment of daytime outdoor comfort levels in and outside the urban area of glasgow, uk. *International journal of biometeorology* 57, 521–533.
- Kruger, E.L., Drach, P., 2017. Identifying potential effects from anthropometric variables on outdoor thermal comfort. *Building and Environment* 117, 230–237.
- Kullback, S., Leibler, R.A., 1951. On information and sufficiency. *The annals of mathematical statistics* 22, 79–86.
- Lazos, D., Sproul, A.B., Kay, M., 2014. Optimisation of energy management in commercial buildings with weather forecasting inputs: A review. *Renewable and Sustainable Energy Reviews* 39, 587–603.
- Lei, B., Janssen, P., Stoter, J., Biljecki, F., 2023. Challenges of urban digital twins: A systematic review and a delphi expert survey. *Automation in Construction* 147, 104716. doi:10.1016/j.autcon.2022.104716.
- Li, J., Heap, A.D., 2011. A review of comparative studies of spatial interpolation methods in environmental sciences: Performance and impact factors. *Ecological Informatics* 6, 228–241.
- Li, J., Liu, N., 2020. The perception, optimization strategies and prospects of outdoor thermal comfort in china: A review. *Building and Environment* 170, 106614.
- Lin, J., Brown, R.D., 2021. Integrating microclimate into landscape architecture for outdoor thermal comfort: a systematic review. *Land* 10, 196.
- Liu, P., Zhao, T., Luo, J., Lei, B., Frei, M., Miller, C., Biljecki, F., 2023. Towards human-centric digital twins: Leveraging computer vision and graph models to predict outdoor comfort. *Sustainable Cities and Society* 93, 104480. doi:10.1016/j.scs.2023.104480.
- Ma, J., Ding, Y., Cheng, J.C., Jiang, F., Wan, Z., 2019. A temporal-spatial interpolation and extrapolation method based on geographic long short-term memory neural network for pm2. 5. *Journal of Cleaner Production* 237, 117729.
- Maćkiewicz, A., Ratajczak, W., 1993. Principal components analysis (pca). *Computers & Geosciences* 19, 303–342.
- Maronga, B., Gryschka, M., Heinze, R., Hoffmann, F., Kanani-Sühring, F., Keck, M., Ketelsen, K., Letzel, M.O., Sühring, M., Raasch, S., 2015. The parallelized large-eddy simulation model (palms) version 4.0 for atmospheric and oceanic flows: model formulation, recent developments,

- and future perspectives. *Geoscientific Model Development* 8, 2515–2551.
- Mathiesen, P., Kleissl, J., 2011. Evaluation of numerical weather prediction for intra-day solar forecasting in the continental united states. *Solar Energy* 85, 967–977.
- Megahed, Y., Shaker, A., Yan, W.Y., 2021. Fusion of airborne lidar point clouds and aerial images for heterogeneous land-use urban mapping. *Remote Sensing* 13, 814. URL: <http://dx.doi.org/10.3390/rs13040814>, doi:10.3390/rs13040814.
- Meng, Q., Liu, Z., Borders, B.E., 2013. Assessment of regression kriging for spatial interpolation—comparisons of seven gis interpolation methods. *Cartography and geographic information science* 40, 28–39.
- Mocanu, D.C., Mocanu, E., Stone, P., Nguyen, P.H., Gibescu, M., Liotta, A., 2018. Scalable training of artificial neural networks with adaptive sparse connectivity inspired by network science. *Nature communications* 9, 2383.
- Moradi, M., Dyer, B., Nazem, A., Nambiar, M.K., Nahian, M.R., Bueno, B., Mackey, C., Vasantha Kumar, S., Nazarian, N., Krayenhoff, E.S., et al., 2021. The vertical city weather generator (vcwg v1. 3.2). *Geoscientific Model Development* 14, 961–984.
- Naikoo, M.W., Islam, A.R.M.T., Mallick, J., Rahman, A., et al., 2022. Land use/land cover change and its impact on surface urban heat island and urban thermal comfort in a metropolitan city. *Urban Climate* 41, 101052.
- Nedd, R., Light, K., Owens, M., James, N., Johnson, E., Anandhi, A., 2021. A synthesis of land use/land cover studies: Definitions, classification systems, meta-studies, challenges and knowledge gaps on a global landscape. *Land* 10, 994.
- Tootkaboni, M., Ballarini, I., Zinzi, M., Corrado, V., 2021. A comparative analysis of different future weather data for building energy performance simulation. *Climate* 9, 37.
- Quemada-Villagómez, L., Miranda-López, R., Calderón-Ramírez, M., Navarrete-Bolaños, J., Martínez-González, G., Jiménez-Islas, H., 2021. A simple and accurate mathematical model for estimating maximum and minimum daily environmental temperatures in a year. *Building and Environment* 197, 107822.
- Schinasi, L.H., Benmarhnia, T., De Roos, A.J., 2018. Modification of the association between high ambient temperature and health by urban microclimate indicators: A systematic review and meta-analysis. *Environmental research* 161, 168–180.
- Schoenberg, I.J., 1973. Cardinal spline interpolation. SIAM.
- Senin, P., 2008. Dynamic time warping algorithm review. *Information and Computer Science Department University of Hawaii at Manoa Honolulu, USA* 855, 40.
- Topalar, Y., Blocken, B., Maiheu, B., Van Heijst, G., 2017. A review on the cfd analysis of urban microclimate. *Renewable and Sustainable Energy Reviews* 80, 1613–1640.
- United Nations, 2019. World urbanization prospects: The 2018 revision. united nations department of economic and social affairs. Population Division, New York .
- Van Houdt, G., Mosquera, C., Nápoles, G., 2020. A review on the long short-term memory model. *Artificial Intelligence Review* 53, 5929–5955.
- Vinayak, B., Lee, H.S., Gedam, S., Latha, R., 2022. Impacts of future urbanization on urban microclimate and thermal comfort over the mumbai metropolitan region, india. *Sustainable Cities and Society* 79, 103703.
- Vivekananda, G., Swathi, R., Sujith, A., 2021. Multi-temporal image analysis for lulc classification and change detection. *European journal of remote sensing* 54, 189–199.
- Wang, W., Li, S., Guo, S., Ma, M., Feng, S., Bao, L., 2021. Benchmarking urban local weather with long-term monitoring compared with weather datasets from climate station and energyplus weather (epw) data. *Energy Reports* 7, 6501–6514.
- Watson, D., Philip, G., 1984. Triangle based interpolation. *Journal of the International Association for Mathematical Geology* 16, 779–795.
- Wei, R., Song, D., Wong, N.H., Martin, M., 2016. Impact of urban morphology parameters on microclimate. *Procedia Engineering* 169, 142–149.
- Wu, X., Hou, J., Hui, J., Tang, Z., Wang, W., 2022. Revealing microclimate around buildings with long-term monitoring through the neural network algorithms. *Buildings* 12, 395.
- Wu, X., Liu, J., Li, C., Yin, J., 2020. Impact of climate change on dysentery: scientific evidences, uncertainty, modeling and projections. *Science of The Total Environment* 714, 136702.
- Xie, Y., Ishida, Y., Hu, J., Mochida, A., 2022. A backpropagation neural network improved by a genetic algorithm for predicting the mean radiant temperature around buildings within the long-term period of the near future, in: *Building Simulation*, Springer. pp. 473–492.
- Yang, S., Wang, L.L., Stathopoulos, T., Marey, A.M., 2023. Urban microclimate and its impact on built environment—a review. *Building and Environment* , 110334.
- Zargar, S., 2021. Introduction to sequence learning models: Rnn, lstm, gru. no. April .
- Zeren Cetin, I., Varol, T., Ozel, H.B., 2023. A geographic information systems and remote sensing-based approach to assess urban micro-climate change and its impact on human health in bartin, turkey. *Environmental Monitoring and Assessment* 195, 540.
- Zhang, J., Li, Z., Wei, Y., Hu, D., 2022a. The impact of the building morphology on microclimate and thermal comfort-a case study in beijing. *Building and Environment* 223, 109469.
- Zhang, J., Zhang, F., Gou, Z., Liu, J., 2022b. Assessment of macroclimate and microclimate effects on outdoor thermal comfort via artificial neural network models. *Urban Climate* 42, 101134.
- Zhang, M., Zhang, X., Guo, S., Xu, X., Chen, J., Wang, W., 2021. Urban micro-climate prediction through long short-term memory network with long-term monitoring for on-site building energy estimation. *Sustainable Cities and Society* 74, 103227.